Application of X-ray Computed Tomography for Assessment of Additively Manufactured Products

To my parents for their supports, encouragements, and sacrifices

تقدیم به پدر و مادر عزیزم

ÖREBRO UNIVERSITY

AMIR REZA ZEKAVAT

Application of X-ray Computed Tomography for Assessment of Additively Manufactured Products

Abstract

Amir Reza Zekavat (2019): Application of X-ray Computed Tomography for Assessment of Additively Manufactured Products. Örebro studies in Technology 85.

Additive Manufacturing (AM) is a novel method for fabricating parts from three-dimensional model data, usually by joining materials in layer upon layer fashion. The freedom of design in this method has resulted in new possibilities for fabrication of parts with complex geometries. Manufacturing near-net-shape parts as well as geometrically complex components such as periodic cellular structures that are used in lightweight structural components, has made AM a promising manufacturing method in industry.

Despite the numerous advantages of the AM methods, the imperfections associated with the manufacturing processes has limited the application of additively manufactured parts. Porosity and surface texture of AM parts especially those fabricated using Laser Powder Bed Fusion (LPBF) methods, have been studied in this thesis. It was observed that the mentioned imperfections have a considerable impact on the mechanical performance of thin-wall structures that are the constituting units of surface-based periodic cellular structures. The quality of internal structure in components fabricated using Fused Deposition Modelling (FDM) and its effect on the strength of those components were the other issues investigated in this thesis.

In order to investigate the mechanical strength of AM parts, as the result of mentioned mesoscale imperfections, appropriate evaluation methods that are capable of quantitatively assessing these imperfections are required. X-ray Computed Tomography (CT), a non-destructive evaluation method, has shown high capabilities for providing useful and reliable geometrical information of both internal and external features of AM components. The challenges involved with the application of CT for assessment of AM component are also studied in this thesis.

Apart from the contributions of this thesis on how CT may be used in AM field, t he r esults o f t his t hesis h as p rovided i nsight i nto t he d esign p rocess of cellular structures. This thesis has provided essential information about the strength dependency of thin-walls as the result of mesoscale fabrication defects and how these defects are dependent on the selected material and design of the structure.

Keywords: Additive manufacturing, X-ray computed tomography, Surface roughness.

Amir Reza Zekavat, Department of Mechanical Engineering
Örebro University, SE-701 82 Örebro, Sweden, amirreza.zekavat@oru.se

Acknowledgements

First of all, thanks to SWEDEN and the Swedish educational system which provided me with such an excellent opportunity to carry out my Masters and Ph.D. education. I want to convey my special thanks to my supervisor Prof. Lars Pejryd, for his trust and giving me the opportunity to do my Ph.D. studies and his consistent support and patience during this period.

I consider myself fortunate and highly privileged to have been born into a family that highly prioritizes education. Thanks to my parents, who have played an essential role by providing all I needed to reach my goals. I am extremely grateful for their unconditional support, sacrifices, and encouragement throughout different steps of my life. Thanks to my close friends at Örebro, especially Ravi Teja, who were like my family and did not let me feel alone while being far from home. Finally, the special thank goes to *Louloudi mou* for standing by my side and being patient, especially at the very end of this journey!

Thanks to those who have technically contributed to this thesis: Carsten Gundlach at imaging facility at Technical University of Denmark (DTU), my co-authors at Research Institutes of Sweden (RISE), specially Pooya Tabibzade and finally Hadi Banaee for his help during the preparation of the thesis. Thanks to Anton Jansson for being a nice office-mate for nearly five years, for our philosophical discussions and his contributions to the theory of:

<div align="center">

Nothing Is Perfect (NIP).

</div>

Finally, it was a great pleasure to work in an international working environment, interacting with people from all around the world. Thanks to the doctoral candidates and researchers at Örebro University, especially those at the mechanical engineering department and the center of Applied Autonomous Sensor Systems (AASS). For me, this was a fun, real-life "The Big Bang Theory" experience, having many Sheldons, Leonards, Rajs, and Howards around me all the time!

Örebro

Summer 2019

آن کس که بداند و بداند که بداند

اسب خرد از گنبد گردون بجهاند

آن کس که بداند و نداند که بداند

آگاه نمایید که بس خفته نماند

آن کس که نداند و بداند که نداند

لنگان خرک خویش به منزل برساند

آن کس که نداند و نداند که نداند

در جهل مرکب ابدالدهر بماند

List of Publications

Paper I: Anton Jansson, <u>Amir Reza Zekavat</u>, and Lars Pejryd, **Measurement of Internal Features in Additive Manufactured Components by the use of Computed Tomography**. *Digital Industrial Radiology and Computed Tomography Conference (DIR 2015)*, Ghent, Belgium, 22-25.

Zekavat made significant contributions to the planning and performing the experimental work.

Paper II: <u>Amir Reza Zekavat</u>, Anton Jansson, Joakim Larsson, and Lars Pejryd, **Investigating the effect of fabrication temperature on mechanical properties of fused deposition modeling parts using X-ray computed tomography**. *The International Journal of Advanced Manufacturing Technology*, 100.1-4 (2019): 287-296.

Zekavat made significant contributions to the experimental work, performed all the analysis and almost all the writing.

Paper III: <u>Amir Reza Zekavat</u>, Anton Jansson, Carsten Gundlach, and Lars Pejryd, **Effect of X-ray Computed Tomography Magnification on Surface Morphology Investigation of Additive Manufacturing Surfaces**. In *8th Conference on Industrial Computed Tomography (iCT2018)*, Wels, Austria, 2018.

Zekavat performed all of the planning, major part of experimental work, all the analysis and writing.

Paper IV: <u>Amir Reza Zekavat</u>, Lars Pejryd, and Carsten Gundlach, **Effect of X-Ray Computed Tomography Magnification on Porosity Analysis of Additively Manufactured Parts**. *World Congress on Powder Metallurgy (WPM18)*, Beijing, China, 2018.

Zekavat performed all of the planning, major part of experimental work, all the analysis and the writing.

Paper V: <u>Amir Reza Zekavat</u>, Pooya Tabib Zadeh Adib, Pär Johannesson, Patrik Karlsson, Torsten Sjögren, Lars Pejryd, **An experimental approach to investigate the influential parameters on mechanical strength of AlSi10Mg thin-wall structures manufactured by selective laser melting**. Submitted to *Journal of Materials Engineering and Performance*, 2019.

Zekavat made significant contributions to the planning and the experimental work, all the CT work, post analysis of the results and the major part of the writing.

Paper VI: <u>Amir Reza Zekavat</u>, **Surface Characterization of Additively Manufactured AlSi10Mg and Ti6Al4V thin-wall Structures using X-Ray Computed Tomography**. Manuscript to be submitted to Journal of *Additive Manufacturing*

Zekavat performed all of the planning, analysis and experimental work and the writing.

Other publications that are not included in this thesis:

Anton Jansson, Jens Ekengren, <u>Amir Reza Zekavat</u>, Lars Pejryd, **Effects of X-ray penetration depth on multi material computed tomography measurements**. In *6th Conference on Industrial Computed Tomography (iCT 2016)*, Wels, Austria, 2016.

Contents

Chapter 1
Introduction

1.1 Background and Motivation

The world's population is growing at a much faster rate than ever before. According to a study conducted by the United Nations (UN), the world's population is expected to increase by 2 billion persons in the next 30 years, from 7.7 billion currently to 9.7 billion in 2050 and increase to nearly 11 billion by the end of the current century [1]. This growth poses many challenges to the Sustainable Development Goals defined by the UN [2]. Moreover, it is a potential threat for exploiting natural resources, including energy, water, and raw materials due to severe economic competition for more production. Since most of these resources are limited and non-renewable, improper use of them causes significant damages to the environment. The recent extreme weather conditions, the frequent natural disasters, and the melting of glaciers are just a few examples caused by global climate change. If the impacts of these environmental deteriorations are not given the much-needed attention, soon we may pass the point that the situation can be reversed. Luckily, many national and international organizations around the world have shown their concerns regarding these issues by taking the initiative and implementing strategic road maps and agendas. These organizations, such as the European Union (EU) continuously set tougher goals and targets to be achieved in order to control the situation. The framework programs for funding research, technological development, and innovation such as "*Horizon 2020*" and "*Horizon Europe*" are the sustainable development approaches for implementing the European environmental research and innovation policies.

As an example, according to the European Environment Agency (EEA), in 2016, the transport sector contributed 20% of total EU greenhouse gas emissions with the road transport accounting for more than 72% of it [3]. Thus, the EU has set tough emission limits for passenger cars. According to the EU's requirements, the passenger cars carbon dioxide emission should not be more than 95 grams per kilometer by 2020. The target set for 2030 for the long-

distance freight transport is to achieve 40% improvement in energy efficiency compared to 2010 [4]. Traditionally, within the field of engineering and production, these goals can be achieved by reducing weight, shortening the production lead time or using light-weight high-performance materials or solutions. The wide application of new composite materials such as Carbon Fibre-Reinforced Polymers (CFRP) which have relatively low weight and high strength is a good example of this trend. Multi-material solutions by combining these polymers with metallic materials such as Aluminum or steel has gained popularity, especially in the automotive industry. The other approaches are the application of mixed material systems or creative lightweight design solutions such as Topology Optimization (TO) tools. Furthermore, innovative approaches for implementing multi-function designs are the most innovative methods which fit in this context. In these lines of thought, two or multiple purposes or requirements are fulfilled in one design. Development of multi-functional structural batteries is an excellent example of this approach, where the body of a car simultaneously carries the mechanical loads and stores the electrical energy [5].

Teknikföretagen, the Association of Swedish Engineering Industries, has proposed a strategic agenda for innovation in production [6]. According to this agenda, the "*Environmentally sustainable production*" and the "*Flexible manufacturing processes*" are the two out of six key areas which can strengthen production in Sweden. Most of the challenges explained in these two areas can be overcome by using new technologies such as Additive Manufacturing (AM). AM technologies are not only beneficial for efficient use of raw materials, fabrication of lightweight components or remanufacturing purposes, but also shorter lead time can be achieved using these methods. They also have a high level of customization, which is suitable for coping with modification of products due to the rapidly growing number of innovative products. High level of flexibility is another enabler of these methods for dealing with external changes such as market development, energy, and environmental crises, and changes in the availability of raw materials [6].

The capabilities of these new manufacturing technologies have brought new possibilities in many different fields of science and technology. As mentioned earlier, developing and investigating on these technologies is considered in the subcategories of many national strategic agendas and regional research funding frameworks. The fact that they are considered in megatrends such as "*Digitalisation*" or roadmaps such as "*Industry 4.0*", the innovative German strategies within the field of manufacturing technologies and processes, shows the level of their importance and the reason for being investigated as it is performed in this thesis.

1.2   Problems and Objectives

AM technologies are newly emerged fabrication processes which have defined a new paradigm in the field of manufacturing. The capabilities of these technologies for fabrication of near-net-shape parts or parts with high geometrical complexity has increased their applications [7]. AM is growing at a fast pace by being more and more implemented in various fields of science and technology, thanks to their potential for fabrication of metallic and non-metallic parts [8, 9, 10, 11]. The investments and the rise in the number of research publications are other metrics revealing the importance of these technologies. Although these technologies are becoming more common, they are still under development and are not very well established compared to conventional manufacturing processes.

There are challenges which hinder the application of AM technologies for being competitive compared to the conventional manufacturing processes. Apart from the financial perspective, there are technical limitations such as dimensional accuracy of parts, especially due to the surface morphology or possible part distortions. Besides, due to layer by layer build-up principle of these methods, porosity is an inevitable phenomenon in the components fabricated using these methods. Such challenges require the application of appropriate inspection tools in order to investigate the quality and reliability of the manufactured components. These inspection tools are not only beneficial for quality assessment of the components, but also for discovering the limitations of the manufacturing processes and how they can be improved. Therefore, inspection using the right inspection tools is an essential step in the AM manufacturing process chain, for obtaining highly robust components and a more reliable manufacturing method.

X-ray Computed Tomography (CT) is a well-recognized inspection method for obtaining the geometrical information of objects and components. Although this method has been used for medical purposes, the industrial application of it is in the early stages. The ability of this method for non-destructively investigation of external as well as internal features of an object makes it a promising tool for investigation of geometrically complex AM components. Despite the outstanding capabilities of the CT, there are limitations and challenges associated with the application of this method, which requires more investigations. This thesis tries to show the importance of CT as a non-destructive inspection tool in the AM production chain for improvement of both the components and the process while considering the challenges and limitations of CT. The general flow of AM production chain and the CT as an inspection method at the end of the chain is shown in Figure 1.1.
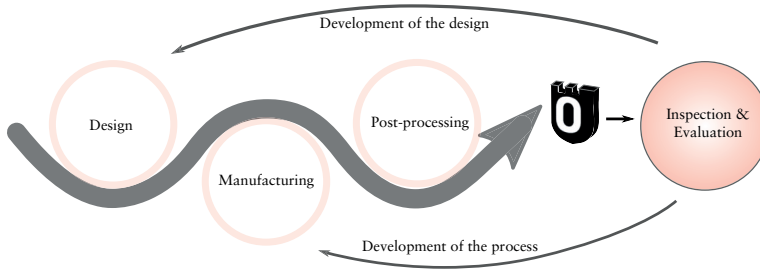
Figure 1.1: Additive Manufacturing chain and the need for inspection methods.

1.3   Aim of the Thesis

The ultimate goal of the research studies performed in this thesis is to provide an insight for improving the AM components quality and consequently their strengths by using CT in the AM process chain as shown in Figure 1.1. To do so, we need to have better background knowledge and understanding of these processes' limitations and capabilities. A prerequisite in this procedure is to be able to quantitatively assess the imperfections and undesired phenomena caused due to the manufacturing processes. This initially requires the application of an appropriate method or tool for characterization of the problem. Secondly, a thorough understanding of how these tools should be used based on their capabilities, limitations, and their associated challenges is required. The aims of this thesis and the corresponding conducted research studies are mainly formed around the following fundamental questions:

How can the imperfections in AM components associated with the process of fabrication be quantitatively investigated?

which leads to the following question:

How can X-ray Computed Tomography be used for the improvement of additively manufactured components and possibly the development of the process?

The other main question which is concerned in these studies is:

How can the imperfections in AM components associated with the process of fabrication influence the quality and potentially the mechanical performance of an AM component?

1.4 Contributions

This section explains how each publication has contributed to answering the above-mentioned research questions.

Paper I addresses the limitations of an AM method by presenting the capabilities and accuracy of the method for generating internal features and how the material and the limitations of the method can impact both the quality of the features and the measurement of CT results.

Paper II provides information on how CT may be used for investigating the quality of AM components and how the CT data in combination with mechanical tests can reveal the strength dependency of AM components on the imperfections generated as a result of the fabrication process.

Paper III and IV address how CT and its limitations associated with the parameter selection and the procedure may influence the quantitative assessment of imperfections in an AM component.

Paper V provides essential information for the development of surface-based periodic cellular (network) structures by presenting how the mechanical strength of AM thin-wall components can be limited due to their imperfections caused by the process of manufacturing.

Paper VI provides essential information on how the quality of thin-wall AM structures is affected as the result of the manufacturing process and the material. These results in combination with the results of *Paper V* can be used for the design of the surface-based periodic cellular structures and the evaluation of the mechanical strength of these structures. Presenting the challenges involved in the quantitative characterization of AM surfaces for better estimation of their strength and suggesting a different approach for characterizing and quantitatively presenting of the surface texture are other contributions of *Paper VI*.

This thesis is the result of a multidisciplinary approach in order to answer practical industrial questions regarding AM products. Various fields of engineering have contributed to form the investigations presented in the publications of this thesis. Figure 2.3 shows how each paper has benefited and contributed to these fields.
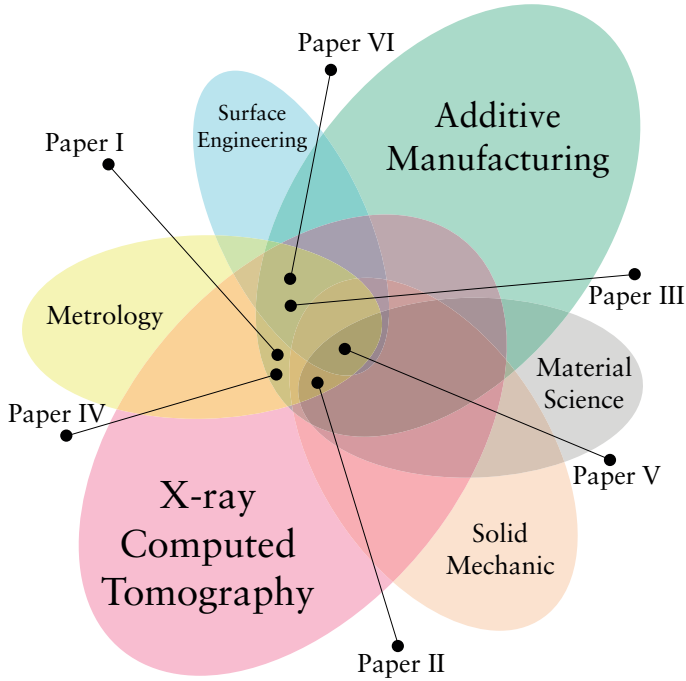
Figure 1.2: The graphical illustration of domains used in this thesis and how each publication fits in these domains.

1.5   Thesis Outline

The rest of the thesis is presented as follows:

Chapter 2 defines the fundamental of the methods, including AM and CT. The chapter follows by explaining the limitations of the methods and a short overview of state of the art. The chapter ends by presenting the experiments and materials used in this thesis.

Chapter 3 presents the results obtained in the publications and the corresponding discussions, presenting how CT as a non-destructive tool has helped to assess the imperfections of AM such as surface texture and porosity.

Chapter 4 provides a summary of concluding remarks and follows with providing insight to the future perspective of the research in this field, the challenges which should be further investigated and possible paths to follow.

Chapter 2
Methods and Experiments

2.1 Additive Manufacturing

Additive manufacturing (AM) is a newly emerged manufacturing technique which has brought many possibilities in the field of manufacturing. AM, also known as rapid prototyping, 3D printing or free form fabrication, which are used interchangeably in this thesis, is a promising method for fabrication of prototypes or parts with complex geometries which are expensive or impossible to manufacture using conventional methods. Based on the definition of American Society for Testing and Materials (ASTM International) and ISO, AM is: *a process of joining materials to make parts from 3D model data, usually layer upon layer, as opposed to subtractive manufacturing methodologies and formative manufacturing methodologies* [12].

AM technologies can be categorized into different subcategories depending on the method of deposition, type or state of the material and type of the heat source for melting the material. There are also many different terminologies for these subcategories which are used interchangeably in the literature. Figure 2.1 shows an overview of available AM methods categorized based on the state of the raw material. Despite the numerous available methods within the field of AM, this thesis focuses only on two of AM methods, Laser Powder Bed Fusion (LPBF) and Fused Deposition Modelling (FDM) which are further explained in the following sections.

The capability of AM methods for fabrication of near-net-shape geometries directly from 3D Computer-Aided Design (CAD) data has made them unique options for manufacturing of industrial components. Moreover, the freedom of design for fabrication of complex geometries has caused a significant growth in the application of these methods in for industrial applications [7]. There is a great interest in the application of AM in various branches of the industry, specifically aerospace engineering [13]. Remanufacturing or repairing of damaged components such as turbine blades instead of replacing them is another cost-effective approach enabled by AM in the aerospace industry [14]. It is also
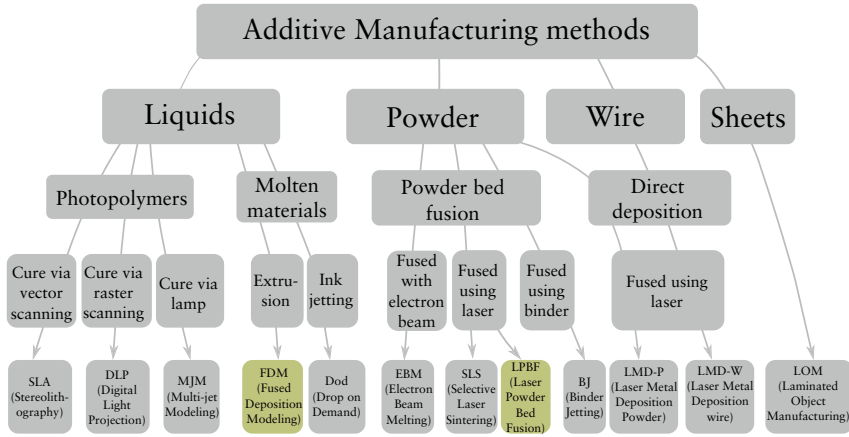
Figure 2.1: Different Additive Manufacturing methods.

a common practice to deposit material using Laser Metal Deposition-Powder (LMD-P) also known as Directed Energy Deposition (DED) as well as Laser Metal Deposition-Wire (LMD-W) to create features such as duct flanges on the large semi-finished aerospace component such as jet engine housings [15]. AM can be used for modifying or repairing of hot forging tools or sheet metal forming dies for car body manufacturing that providing a new exterior design of a car in a short period of time is desired [16]. Shortening the lead time by substituting multiple manufacturing methods by one is another benefit of AM. For example, multiple machining processes in addition to assembly or joining processes such as welding can be substituted by one AM process with possibly a minor post-process such as surface or heat treatment. Besides, many materials which are used, especially in the aerospace industry such as Titanium alloys have poor machinability, and 3D printing of them in some cases is favorable.

The freedom of design brought by AM has been extremely beneficial for the fabrication of lightweight metallic components. Using the powder bed methods, metallic structures with low apparent (relative) density with the help of periodically repeated miniature struts or thin-wall surfaces can be manufactured [17, 18, 19]. These structures can be used for lightweight structural and shock absorbing applications, the same way that metallic foams and porous metals have been used [20, 21, 22]. The main difference between these structures is that they consist of structured periodic cells. By controlling the unit cell size as well as the thickness or diameter of the wall or struts which can be in the range of a tenth of mm, various relative densities can be achieved. These low relative-density periodic architected designs gain a significantly high stiffness which has opened new possibilities for various industrial applications [23, 24].
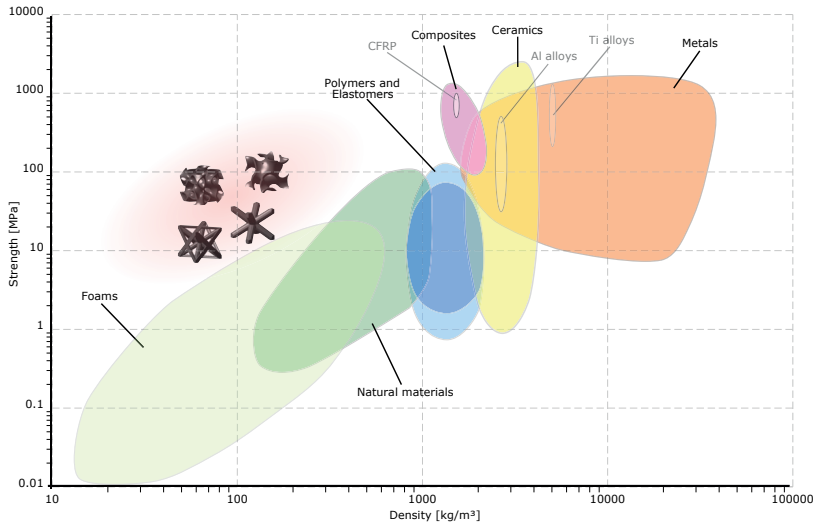
Figure 2.2: Strength versus density chart for material selection suggested by Ashby and strut and surface-based unit cells courtesy of Panesar et al. [17].

Figure 2.2 presents the stiffness versus density chart for material selection provided by Ashby and the placement of low density, high stiffness periodic cellular (network/lattice) structures (strut and surface-based) in the top left of this chart which is considered as "*Search Region*" in this book [25]. In literature, these structures are also called as "functionally graded lattice structures". Various surface-based structures can be made with the help of Triply Periodic Minimal Surfaces (TPMS) which have gained considerable attention recently. The unique privilege of these structures is the result of their controlled architecture which can be obtained with the help of AM and be used for the design of lightweight structures or infill design of structural parts as shown in Figure 2.3. As it is shown by varying the thickness of the walls in the cellular structure, various relative densities can be achieved. *Paper V* and *Paper VI* provide useful information for the design of these structures by respectively investigating the effect of designed thickness variation on the mechanical strength and as-built dimensional accuracy of the thin-wall structures.

Despite the mentioned advantages, AM has not been widely used for the production of metallic parts as compared to the other conventional manufacturing processes. One of the crucial reasons is the relatively high cost of production using powder bed AM methods. Other limitations are related to the quality of parts, for example, the high surface roughness resulting in poor dimensional accuracy especially in case of periodic cellular structures where the surface roughness can affect the strength of the component. Porosity and parts
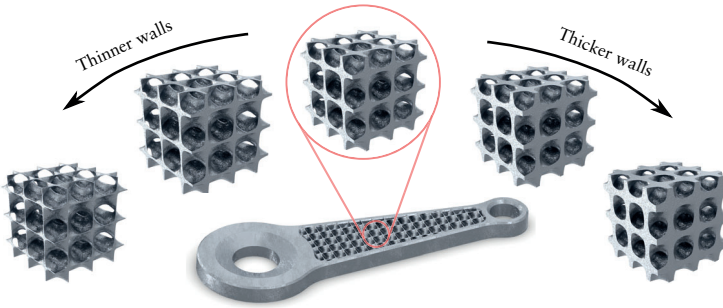
Figure 2.3: A part with surface-based Periodic Cellular Structure infill and the possible thickness variation of the walls in the cells.

distortions due to residual stresses are other factors limiting the application of powder bed AM methods to only specific cases. In the following sections, the manufacturing methods used in this thesis and their limitations are discussed in more details.

2.2   Laser Powder Bed Fusion

Laser powder bed fusion is referred to the powder bed methods that use a high-intensity laser beam as the energy source for melting the powder. Selective Laser Melting (SLM) is interchangeably used to refer to this process. However, SLM is a trademark of SLM Solutions GmbH, and LPBF is a better choice for referring to this method. In this method, a micro-scale high layer of powder is spread on the built plate. Using a focused laser and a scanning unit, the powder is melted selectively at locations in a plane according to the geometrical information obtained form slicing of the 3D CAD data. The build plate is moved downward in order to deposit a new layer of powder with the help of a roller. The laser then melts the next layer on top of the previous melted layer according to the CAD data. This process is continued until the full geometry is fabricated. In this process, depending on the material, the build chamber is filled with inert gas in order to avoid oxidation between the layers. Figure 2.4 illustrates a schematic of this method [26].

There are challenges related to this method, which may affect the quality and strength of LPBF components and consequently, their application in the industry. Since this method consists of repetitive heating and cooling cycles, the microstructure in the 3D printed component is not necessarily homogeneous which in some cases causes residual stresses and severe distortions in the component [27, 28]. The microstructure may also affect the strength of the component, which is partially pinpointed in *Paper V*. This problem can
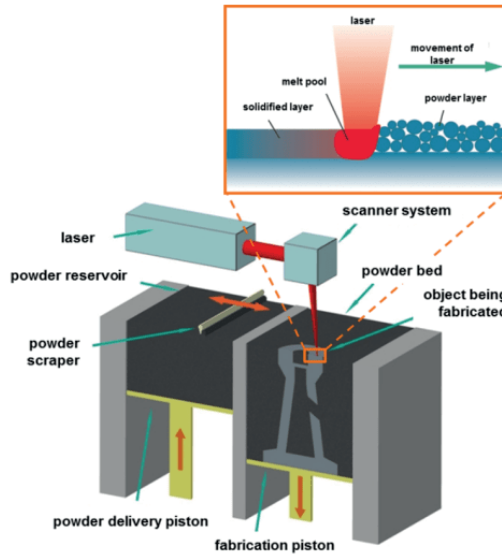
Figure 2.4: Schematic of Laser Powder Bed Fusion process

be highly eliminated by performing the appropriate heat treatment procedure, which relieves the residual stresses [29]. Although the microstructure can have a significant impact on the mechanical strength, studying the effects of the microstructure is out of the scope of this thesis. The other limitations of LPBF are porosity and the surface roughness of the components. The effects of the latter limitations on the mechanical strength of thin-wall components is investigated in *Paper V* and explained in detail in the following sections.

2.2.1 Surface Roughness of LPBF Components

Poor surface finish is a common undesired issue of LPBF as-built components. This is a more significant issue in Electron Beam Melting (EBM) method since the powder is initially sintered at elevated temperature and the size distribution of powder particles as well as layer height are more significant as compared to LPBF [30]. Many parameters such as size distribution of powder particles, the energy density of heat source, the layer height thickness, and the geometry of the component may affect the surface roughness. Calignano et al. studied the effect of process parameters on surface roughness of SLM parts [31]. Besides, up-skin or down-skin side of a feature, as well as the angle of that feature relative to the build direction, has an impact on the surface quality [32, 33]. Although the complexity of the surface can be potentially beneficial in spe-
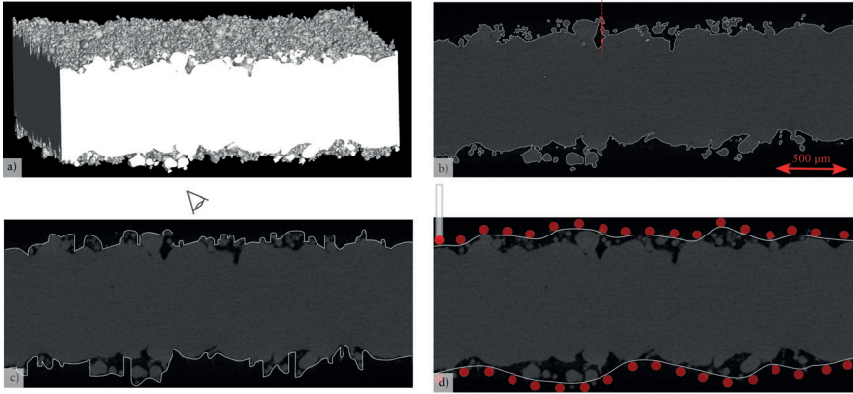
Figure 2.5: a) 3D reconstructed volume of a thin-wall structure b) surface obtained from CT c) schematic of surface obtained from lin-of-sight method d) surface obtained from tactile method

cific cases such as increased heat transfer due to the increased surface area, it is normally considered as a disadvantage. There are research studies which have shown that the tensile strength or fatigue performance of AM parts can be influenced by the AM surfaces [34, 35, 36]. This issue can be eliminated or minimized using electrochemical polishing and chemical etching as well as mechanical post-processing such as shot peening or blasting [37, 33, 31, 38]. However, these methods are not effective or possible in many cases where the surfaces are not accessible for example in parts with internal features such as long conformal cooling channels or periodic cellular (lattice) structures used as infill pattern of lightweight components.

Another critical issue regarding AM surfaces is how to investigate and present them quantitatively. There are many studies which have used Coordinate Measuring Machine (CMM) for evaluating and measuring AM surfaces [39, 40]. Due to the complexity of these surfaces, such as size and shape of features at the peaks or deep valleys, even using the smallest CMM probes cannot result in a correct acquisition of surface information. Also, there are numerous studies which have used non-contact optical methods such as focus variation microscopy and optical profilometry which are also inappropriate methods for detailed surface characterization of AM surface since the sub-surface cavities (re-entrant features) and valleys cannot be captured using these line of site methods [41, 42, 38]. Figure 2.5 a shows a 3D reconstructed volume of a thin-wall structure. Figure 2.5 b shows the surface obtained form CT for a selected cross-section. Figure 2.5 d and c schematically show illustrates how the contact and line of sight methods do not provide the true information of an AM surfaces and can lead to wrong information when the surface details are essential.

Apart from the studies in which the inappropriate tools for surface characterization are used, there are other studies where CT has been used for this purpose. However, despite using CT for surface investigations, insufficient CT resolution (voxel size) was used which does not lead to resolving the surface features which are in smaller size range as compared to the used resolution [43]. Therefore, the investigations in *Paper III* were performed to present how CT resolution can affect the measurement of surface features and which resolution should be used for resolving these micro-scale surface features.

There are other studies which have used CT for surface characterization, but inappropriate surface parameters such as "amplitude parameters" (Ra, Sa) were used to present the surface roughness [44, 45, 39]. Ra, specifically cannot reveal and present useful information of an AM complex surface since in an AM surface profile, usually, more than one height value for each length value exists. Although this has been concluded in many studies, since these parameters are historically very well accepted and used in the industry, they are still used in various research studies. To overcome the limitation of Ra in their studies, either the topmost values or the lowermost values among the multiple height values are used, which is a selective method and filters out the surface information. Figure 2.5 b shows the surface line of an AM surface obtained from CT data and how Ra is not useful due to multiple height values in the profile. The "Hybrid parameters" and "3D volume parameters" are recently being used for presenting the surface roughness of AM surfaces which do not have the mentioned limitations of the amplitude parameters and provide detailed information of an AM complex surface when the mesoscale mechanical response of miniature components is of interest. In *Paper VI*, 3D volume parameters (Vmp, Vmc, Vvc and Vvv) based on ISO 25178-2:2012 in combination with material ratio curves are used to investigate and characterize the surfaces of AlSi10Mg and Ti6Al4V thin-wall components [46]. Vmp is material volume in the hill region, Vmc is material volume within the core, Vvc is void volume within the core and Vvv is void volume below the core. Further details of how these parameters, in combination with their corresponding material ratio curves, were used to reflect AM surfaces, can be found in Section 2.5.

2.2.2 Porosity in LPBF Components

Due to layer by layer deposition principle and the dynamics of the melt pool, having lack-of-fusion defects or gas pores is an inevitable phenomenon in LPBF method. By optimizing the process parameters of powder bed methods, the porosity content can be minimized, and very high-density parts are achieved [47, 48]. However, the presence of pores, especially in components with miniature features such as struts or thin walls, can potentially affect the mechanical response of the part [49]. The porosity issue can be eliminated to a large extent by using Hot Isostatic Pressing (HIP) post-treatment, which improves the high cycle fatigue performance of AM components [36]. In HIP high pressure
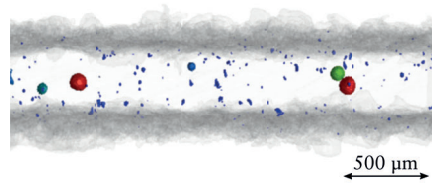
Figure 2.6: Pores in a thin-wall specimen

in combination with elevated temperatures are used to minimize the size of the pores. Despite the capability of HIP process for eliminating the porosity issue, knowing the size of pores, as well as their distribution, especially in a thin-wall or strut component of cellular structure, is essential. The importance of porosity analysis for cellular structures is shown in Figure 2.6. A relatively large pore in a thin-wall component where the diameter of the pore is nearly one third of the wall thickness can be seen. This causes a large local stress concentration, which has a significant impact on the mechanical response of this feature. A detailed porosity analysis on the thin-wall components is presented in *Paper V* and *IV*.

2.3 Fused Deposition Modelling

Fused Deposition Modelling (FDM) also known as Fused Filament Fabrication (FFF) is an extrusion-based AM method. FDM was initially developed and used for prototyping applications. However, nowadays, many structural components are manufactured using this method, and different branches of science and engineering have benefited from it [50, 8]. FDM is probably the most common AM method worldwide, due to the low cost and availability of both the raw material and printers. Low maintenance cost and ease of operating the machines as well as open-source software are other reasons of FDM's popularity. The process is based on extruding the semi-molten material using a nozzle and depositing it on the paths which are created from the slicing of the CAD geometry. The material is pushed into the nozzle using a feeding system before it enters to the liquefier. The nozzle can move in the plane parallel to the build plate for depositing the material in the plane obtained from sliced CAD data. The build plate is moved in the height direction in order to make it possible to deposit the subsequent layer on the layer which is already printed. This process is continued until the final part is fabricated. Figure 2.7 shows a schematic illustration of FDM method. There are two commonly available materials used in FDM, Acrylonitrile Butadiene Styrene (ABS) and polylactic acid (PLA) which the latter used in this thesis. The part accuracy, mechanical strength, and its relation to the build direction of FDM components are studied in various research works [51, 52, 53]. Process parameter optimization studies were carried out to improve the precision of FDM parts [54, 52]. However, the link between the mechanical strength and the internal structure was not reflected in details. Therefore, an in-depth CT investigation of the internal structure and the bond quality of extruded filaments in an FDM part and their impact on the mechanical strength of the part was studied in *Paper II*.
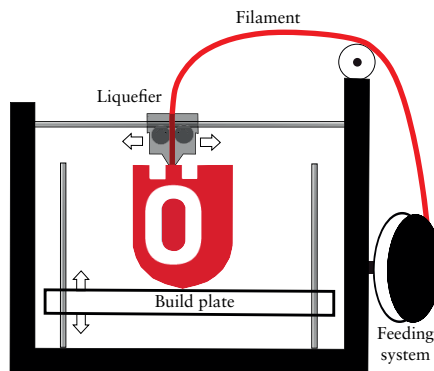

Figure 2.7: Schematic illustration of Fused Deposition Modelling method.

2.4   X-ray Computed Tomography (CT)

X-ray Computed Tomography (CT) is a non-destructive imaging method for evaluation and inspection of objects. The method is based on the ability of X-rays to penetrate the object in order to generate radiographic projections resulted from the attenuated X-rays which have passed through the object. Initially, 2D X-ray radiographic images were used for medical applications. However, In the 1970s, the first medical CT equipment was available due to developments of 3D CT done by the Nobel prize winners, Allan McLeod Cromac and Newbold Hounsfield. Due to low resolution and insufficient accuracy of the method, it was not widely used for industrial applications.

With the improvements in both hardware and software in the last twenty years, CT systems with high capabilities have become available for industrial applications. The current CT systems are used for various purposes ranging from inspection of internal structures to dimensional accuracy of industrial components or even in-line quality controls in food industry [55, 56, 57]. The benefit of CT compared to the conventional metrological methods for examples CMM is that the number of features to be measured does not affect the measuring time with CT [58]. In addition, using CT, it is possible to non-destructively obtain the geometrical information of the internal features of a component which is not possible to be obtained with other measuring systems [59, 60, 61, 62].

2.4.1   CT Procedure

The procedure of obtaining measurement result using CT, on the contrary to many other measuring or inspection tools, consists of multiple essential steps. The appropriate selection of parameters in each step requires a deep understanding of how this method works. Therefore, this section provides a general overview of the steps and influential parameters involved with using CT. The steps and associated parameters start with the generation of X-ray in the tube and end with the measurement performed on the acquired 3D volume. This background knowledge is essential for a better understanding of the possible sources of errors and reliability of the measurements.

X-rays, electromagnetic waves with wavelengths in a range between 0.01 and 10, nm are generated in an X-ray tube. This is done by bombarding the target (anode) by electrons as a result of acceleration voltage generated between cathode and anode in the tube. The main part of the acceleration energy is transferred to heat, and nearly one percent of it is converted into X-rays. The result of the mentioned interaction is a polychromatic X-ray beam which consists of photons with various energy levels. This is due to the fact that the X-ray spectrum is the combination of different radiations which are the "Bremsstrahlung" (braking) radiation, the characteristic radiation and the photons which are the result of accelerated electrons with the nucleus of tar-
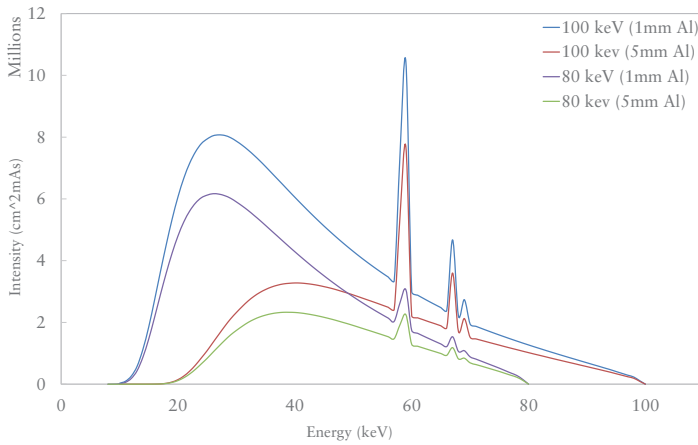
Figure 2.8: X-ray spectra with various energy levels and filter thicknesses.

get's atoms interaction. The polychromatic beam, which is used in nearly all lab CT systems is one of the main limitations of such systems compared to the monochromatic beams used in synchrotron beamlines. The desired X-ray spectrum can be achieved by changing the acceleration voltage, the tube current, and the proper selection of target material and filters. The acceleration voltage, which is considered as the highest energy level of a spectrum defines the ability of X-rays for penetration. In order to increases the ability of the beam to pass through an object with a relatively larger thickness or a high atomic number, a higher tube voltage should be selected. Increasing the acceleration voltage increases the intensity of a spectrum as well. The tube current, on the other hand, only decides the quantity or the intensity of the beam. In other words, increasing the tube current only increases the photon count and not X-rays with higher penetration ability. Choosing proper filter material and thickness can also change the generated spectrum by filtering out the low-level energy rays (Bremsstrahlung) of the spectrum. Finally, since the energy level of characteristic X-ray peaks in a spectrum is the function of the target material, the proper selection of target is vital for obtaining the beam with the desired X-ray spectrum. Figure 2.8 shows different spectra depending on different tube voltages and filters calculated for a tungsten target generated using SpekCalc [63].

The generated X-rays then interacts with the object to be scanned. A part of X-rays is absorbed due to the photoelectric effect with the absorption being proportional to the atomic number of the material to be scanned. Another part of the generated photons interact with the electrons of the atoms, and if the
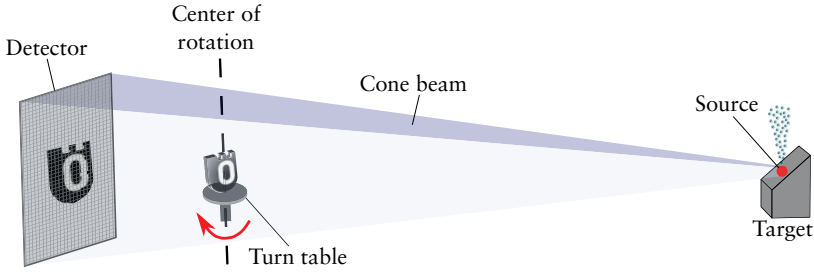
Figure 2.9: Schematic of CT components and process.

energy of the photon is considerably higher than the electron binding energy, they scatter. In this case, which is called Compton scattering, the photon loses a part of its energy, which changes its wavelength and possibly the travel direction as it scatters. Thomson scattering is another phenomenon very similar to Compton scattering with the main difference that the energy level of the photon interacting with the atomic electron and the scattered photoelectron remains the same. The attenuation coefficient of a material is the sum of the above-mentioned phenomena and a key parameter for calculating the total attenuation of X-ray interacting with that material. For a homogeneous object, the total attenuation is calculated using the Beer-Lambert law:

$$I(x) = I_0 e^{-\mu x}$$

where the I_0 is the intensity of X-rays before the interaction, I is the intensity after the interaction, μ is the coefficient of attenuation and x is the distance that X-ray has traveled in the object. The attenuated beam then is converted to visible light after interacting with the scintillating material, usually deposited on the detector sensor. The detector then converts the light to its corresponding electric signal in each pixel. The received signals in the pixels generate a projection of the object, which contains the information of the attenuated rays after interacting with the object. In order to generate a CT dataset, multiple projections should be acquired by rotating the object in a stepwise angular range. The number of projections is decided based on the number of horizontal pixels of the detector used in the field of view. Figure 2.9 below shows a schematic of CT components and process.

The obtained projections, as well as distance of the object (center of rotation) in relation to the detector and the focal spot plus the cone-beam angle, are needed in order to reconstruct a dataset using the commonly used reconstruction algorithm, Filtered Back Projection (FBP) [64]. A set of filters can be used in this step for minimizing the noise related to the method and provide a better representation of the data. Although FBP is the most common reconstruction method in CT, it is a 2D reconstruction method and cannot be used
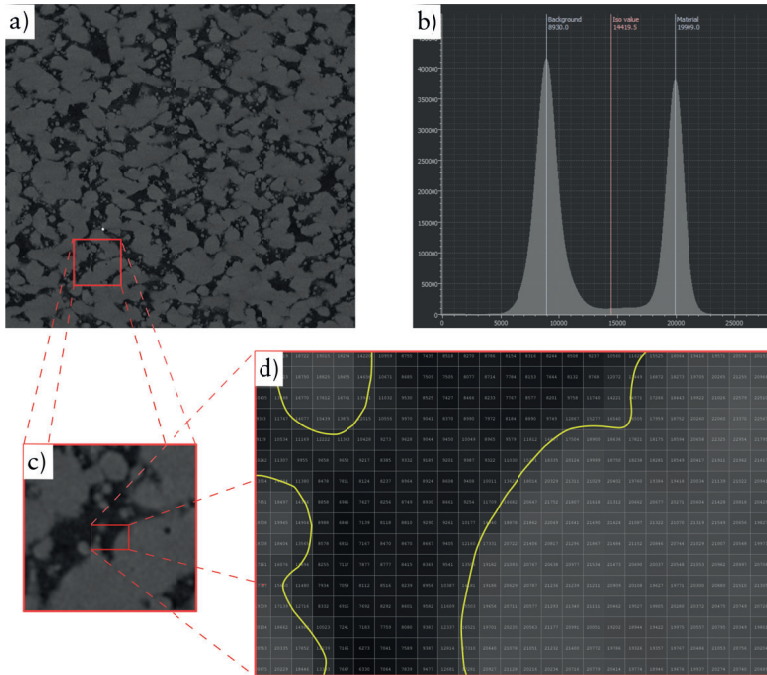
Figure 2.10: a) A cross-section of reconstructed volume containg material and background (air) gray values b) Histogram, material and background peaks and ISO50 threshold c) Close-up of the cross-section d) ISO lines as the result of surface determinataion with sub-voxeling.

for a cone-beam, which is the typical type of beam in industrial CT machines. Therefore, "Feldkamp, Davis and Kress" (FDK) reconstruction algorithm, an advancement to the FBP for 3D reconstruction is used which accounts for the conical shape of the beam by splitting the cone-beam to multiple 2D fan beams and accounting for their effect on every horizontal detector lines. The result of this process is a reconstructed volume consisting of volumetric pixels (voxels) which contain the information of the scanned object in the form of gray values. Figure 2.10 a shows an example of a cross-section from a 3D reconstructed volume in form of gray values. The information of 3D volume can be presented in the form of a dataset containing the number of voxels with particular gray value and can be illustrated using a histogram as shown in Figure 2.10 b.

The next step is data analysis process, which refers to a set of procedures to obtain results from the reconstructed data. Various prepossessing methods, including filtration and smoothing of the dataset, can be used in this stage. The volume then needs to be segmented in order to separate different regions

of it, for example, in a simplified case, air and the material. Threshold-based segmentation methods are the conventional methods for separation of two or more objects in a dataset based on their gray values. These methods are based on defining a threshold gray value of two peaks, usually air and the material. If this threshold value is the mean value of the two peaks, it is called ISO 50 method, which is mainly used in this thesis. By using the sub-voxeling methods, for example, a local threshold to achieve higher resolutions compared to the size of the voxel resulting in a smooth surface determination of two different materials. Figure 2.10 b shows an example of a histogram and how ISO50 segmentation method can separate material peak from the air peak. At this stage, further dimensional analysis can be performed on the 3D volume. It is possible to transfer the 3D volume data into other forms of geometrical information such as point clouds for further analysis, which is the method used in *Paper III*.

2.4.2   Parameters Affecting the Measurements

There are CT parameters which can highly affect the measurement results of a scan. By positioning the sample at different distances relative to the detector and the source, the operator can decide the magnification and consequently, the voxel size of the dataset. Magnification can be obtained by dividing "Source to Detector Distance (SDD)" to the "Source to Object Distance (SOD)". A larger ratio results in higher magnification and smaller voxel size and vice versa. In industry, there might be limitations for having a small SOD usually due to size limitation of the sample. Therefore, the sample should be scanned at lower magnifications, obtaining a dataset with large voxel size, which in turn can impact the measurements. This phenomenon was the main motivation of the studies performed in *Paper III* and *IV*, in which the effects of voxel size on the measurement of porosity and surface features are studied. Figure 2.11 schematically illustrates how magnification can affect the projections.

The rest of this section provides a general overview of the parameters and the error sources which may affect the measurement results obtained using CT. The main reason for presenting this section is to emphasize on the fact that, the main challenge for obtaining reliable measurement results is to have a decent dataset, to begin with. Therefore, a series of steps should be appropriately followed, and proper settings should be selected. Therefore, one should be aware of the consequences of each step and how each setting can impact the final results. In addition, there is no universal standard procedure to be followed for different scans, and each individual scan requires its own unique settings and analysis procedure. The factors affecting the measurements can be categorized into five main groups depending on their impact and the order of their occurrence during a scan.
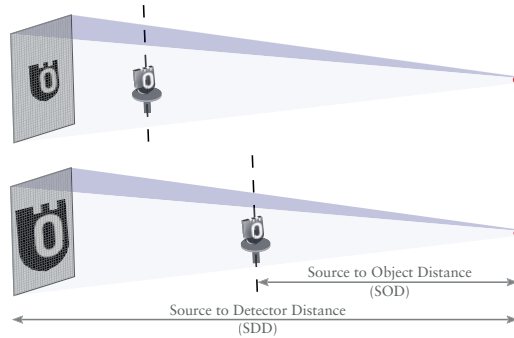
Figure 2.11: Effect of CT magnification.

Limitations of the system: Some of the system's limitations are physical, such as the detector's pixel size. The detector's pixel size, the SOD and SDD are the main parameters which determine the voxel size of a dataset. The focal spot blurring, which is the result of an increase in the size of the focal spot size due to the application of higher energy levels, is another source of error related to the system. Instability of the tube voltage can lead to possible fluctuations of the focal spot, which has a similar blurring effect. The precision of the drive system for positioning the rotary table can also highly impact the source to sample distance, which is crucial for the reconstruction algorithm. The X-ray spectrum and the fact that we use a range of X-ray energies on the contrary to the synchrotron facilities results in a beam hardening artifact. Beam hardening is referred to the phenomenon that the low energy part of the spectrum being absorbed/highly attenuated at the very first layer of the sample to be scanned. Even the tilt of the detector, especially in custom-built industrial systems, can highly affect the measurement results. The detector technology, its sensitivity, and the scintillator material are other parameters which may affect the quality of the data [65].

Data acquisition: The Data acquisition process starts with the selection of energy settings and filters which decides the quality and penetration power of the beam. Inappropriate selection of these parameters results in data which is not reliable for further analysis. For example, selecting too low voltage results in poor penetration and consequently, the dataset will experience photon starvation artifact. In many systems, it is possible to choose between different targets such as Tungsten, Molybdenum, or Copper, which is another crucial factor on the beam specifications. Tungsten is usually used for high absorbing materials such as metals and Molybdenum or Copper for low absorbing materials such as plastics or soft tissues. The flat field correction is another essential procedure which is performed for eliminating the effects of unstable or dead

pixels and potential ring artifacts in the final dataset. There are other parameters such as frame averaging and exposure time per projections which should be wisely chosen. Depending on the texture of the material to be scanned and the purpose of the scan, for example, if porosity is concerned or only external geometrical data. Last but not least, "number of projections", which should be selected based on the number of horizontal pixels used in the field of view should be chosen accordingly. An insufficient number of projections results in unreliable information in the areas of the dataset which are at the furthest distance from the center of rotation [66].

Reconstruction: The process of reconstructing 3D volume from the projections and the selected filters at this stage can play an important role in the quality of the dataset and the measurements. Usually, it is the operator who should select the appropriate beam hardening correction level based on visual inspection of the slices. Based on the purpose of CT investigation, such as porosity analysis or length measurement, the operator may also use various filters such as smoothing, to improve the signal to noise ratio (SNR). It should be mentioned that the filters used at this stage can highly alter or eliminate micro-scale features of a scan such as small pores or the texture of an AM surface. Depending on the reconstruction algorithm, it might be required to manually find the center of rotation or perform a post-alignment process on the projections. Ring artifact, which is a common phenomenon caused due to the reconstructing algorithm, can also be minimized by the operator by choosing appropriate correction setting. Finally, there might be higher levels of uncertainties in the measurements performed on the 3D volume, which are acquired from the very top and very bottom of the fieled of view. This is due to the Feldkamp artifact which itself is the result of the mathematical approximation done in Feldkamp algorithm to account for the conical shape of the beam. Wrong input of the cone angle as a result of inaccurate SOD value, can increase the effect of the uncertainty in the results caused by this artifact.

Geometry, material and environment: The environment, geometry, material, and even the surface roughness of the sample to be scanned, may all impact the measurements [40]. The temperature fluctuations during the scan can also impact the length measurements due to thermal expansion. That is why the metrological CT systems benefit from temperature-controlled chambers. Besides, if a high attenuating material such as metal in combination with low attenuating material should be scanned, scattering and metal artifacts may occur. The effects of these artifacts can be minimized by using algorithms and methods [67]. As an example of the impact of multi-material and geometry complexity, scanning an electronic circuit-board which consist of different metallic materials and unfavorable geometrical aspect ratio is considerably more challenging than scanning a homogeneous precision ruby sphere with very low surface roughness. The stability of the sample on the turntable during the scanning can

also be categorized in this section. If a proper fixture for keeping the sample stable, during the whole scan is not used, motion blur artifact will be inevitable [68]. Vibrations should also be avoided in order to minimize possible motion blur artifact. Even though there are post-alignment methods to minimize this artifact for small movements, it is recommended to use an appropriate method to keep the sample fixed during a scan.

Data analysis: In order to perform any measurement analysis on the 3D reconstructed volume, the materials should be segmented from each other. In a simplified case a volume comprises of voxels with gray values, usually air and the sample. There are various methods for separating or defining a threshold for separation of gray values such as Otsu [69]. As it was explained before, this can be done automatically using a commonly used ISO 50 method; otherwise, the operator can manually decide the threshold by defining the range of gray values associated with each material. A dataset with partially overlapped peaks due to photon starvation artifact or low signal to noise ratio can be challenging for surface determination since there are gray values which can belong to either of the materials. In addition, the available software packages for data analysis, benefit from surface determination algorithms which improve the segmentation by using sub-voxel accuracy [58]. As a result, the surface becomes smoother compared to the segmentation methods without sub-voxeling as shown in Figure 2.10 d. Different software packages use their own proposed algorithms. However, algorithms such as the "Marching Cube" have provided similar solutions before. There are more advanced algorithms for improving the surface determination, such as iterative methods defined as "local adaptive" in VGStudio MAX software, which highly improves the surface determination results. This has great importance, for example, for surface determination of AM complex surfaces and consequently, the measurement results. The registration of 3D data volume against the CAD data for comparison of the as-designed and the as-built component may also affect the measurements as will be pinpointed in chapter 3.

Among the mentioned categories, the errors related to data acquisition and data analysis stage are more operator-dependent as compared to the rest of the error sources. The data acquisition and reconstruction can be ideally automated, for example, aRTist is a reliable simulation tool for proper selection of energy settings as well as the optimal orientation of the sample for the scan [70, 71]. However, the selection of other parameters, especially in data analysis stage requires an experimental knowledge of an operator since there is no standard procedure for most of the mentioned parameters as each scan differs from another one.

2.4.3   Reliability of the CT Measurements

The main purpose of this section is to present the current methods used within the field of industrial CT to overcome or minimize the effect of CT errors in order to increase the repeatability and reliability of the measurements. Different approaches have been investigated and suggested in various research studies [72, 73, 74, 75, 76]. These methods for improving the reliability of the CT measurements can be divided into three groups:

In the first group, the system can be calibrating by implementing the method suggested in VDI/VDE 2630 part 1.3. With the help of reference objects, the length measurement error, and the accuracy of the system can be obtained. The problem with reference objects used for evaluating the accuracy of systems is that they are made of ideal geometries and materials with ideal radiographic properties to minimize CT artifacts. However, scanning objects which have complex geometries or consist of high-attenuating materials or materials causing scattering or severe beam hardening can restrict the applicability of the obtained results.

In the second group, the system is calibrated for a specific setting by using calibrated objects with known distance, scanned at the same magnification at which the sample is going to be scanned. This method which was used in *Paper III*, *IV* and *VI* minimizes the potential errors related to the inaccuracy of the drive system and uncertainties associated to that.

In the third group, the dataset is calibrated using precision objects (or features on/in the sample), which are scanned with the sample in the same scan. It is possible to drill micro-scale holes or put precision spheres on the sample and use the distance between these features which is measured using another calibrated method such as CMM and use that data for calibration of the dataset. In *Paper I* the distance between features manufactured in the test specimen measured using CMM were used to calibrate the 3D volume and *Paper II* calibration spheres with distance measured using CMM was used for the same purpose.

There are other methods for calculating 2D or 3D resolution of a CT system. JIMA phantoms are set of line-pair phantoms for evaluating the resolution in 2D projections as well as calculating the focal spot size of a system [77]. QRM GmbH provides 3D line pair phantoms which can be used for 3D resolution evaluation of CT systems [78]. There are other lab-made reference objects for evaluating the accuracy of a system which can be found in the literature [72].

Besides, in some cases, it is possible to compare the features (or distances between features) of a sample with the data obtained from other measuring methods. This is primarily a useful method when the features to be scanned (or the sample) are tiny and high magnification is required; thus it is practically impossible to fit a reference object in the same scan. For example, in *Paper VI*, the distances between selected spherical partially attached powder particles measured using CT were compared with those of measured in the data obtained
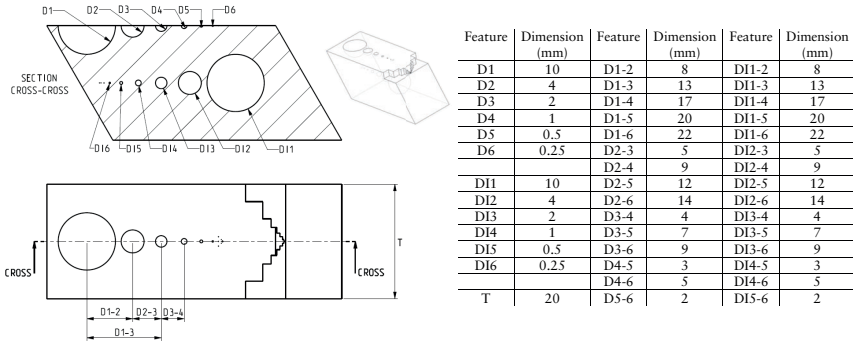
Figure 2.12: CAD design, dimensions and features of the sample geometry used in Paper I.

from SEM. The results of length measurements obtained from CT and SEM were in good agreement. This is obviously not a scientific method of validation or calibration of a dataset. However, it increases the reliability of the results obtained from CT.

2.5 Experiments and Materials

In *Paper I*, a sample geometry was designed to evaluate the accuracy and limitations of an EOS M290 (LPBF method) for the fabrication of both internal and external features. The geometry was made of Ti6Al4V powder provided by EOS GmbH. A Mitutoyo CMM with 1 mm in diameter probe was used to measure the distances between the external half-spheres. The part was scanned using a Nikon XT H 225 system with tungsten target, tube voltage of 218 kV, filament current of 80 µA and 720 projections. The distance between the largest external features was used to calibrate the CT data in VGStudio Max 3.0. The CAD design and the features of the test sample used in this study are shown in Figure 2.12.

The specimens used in *Paper II* were manufactured using black PLA filament with 2.85 ±0.1mm in diameter using an Ultimaker2 FDM printer. The material specifications can be found in [79]. The tensile specimens were manufactured according to the ISO 527 standard [80]. Further details of the specimens, including CAD design and the fabrication orientation in respect to tensile load, are presented in Figure 2.13. All the manufacturing parameters except the temperature remained identical for all the specimens. Different temperatures ranging from 180 °C to 260 °C with 10 °C increment were used resulting in 9 sets of samples. Three samples of each temperature fabrication were manufactured for the tensile testing. 0.8 mm diameter extrusion nozzle, the layer thickness of 0.1 mm, and infill density of 100% was chosen for manufacturing

of the specimens. The build plate temperature and the nozzle travel speed were set to 60 °C and 70 mm/s respectively. A uniaxial tensile test was performed at room temperature using an Instron 4458 instrument with a load cell of 300 kN and at a speed of 1 mm/min. One out of three specimens of each manufacturing temperature was CT scanned using a Nikon XT H 225 micro-computed tomography system. The voltage and amperage of the tube were 80 kV, 81 µA. 1080 projections with an exposure time of 1 second, resulting in a dataset with voxel size of 15.9 µm was used. The post-processing was done using VGStudio MAX 3.0.

A set of 35 mm tall specimens made of AlSi10Mg (Al) and Ti6Al4V (Ti) provided by (EOS GmbH Germany) were manufactured using LPBF which were used in *Paper III*, *IV* and *VI*. The details of chemical composition and mechanical properties of mentioned materials are described elsewhere [81, 82]. Flat thin-walls with thicknesses of 0.4 mm, 0.8 mm, 1.2 mm, 1.6 mm and 2 mm were fabricated. A 0.4mm thin cylinder surrounding the walls was used in order to keep the surfaces of interest untouched and avoid potential distortion of the specimens caused by residual stresses. Both AlSi10Mg and Ti6Al4V specimens were fabricated using 30 µm powder layer height using an EOS M290 [83]. The rest of the parameters were locked for this machine, and it was not possible to change them. Figure 2.15 presents the powder particle size distributions for Al and Ti. The CAD geometries of the specimens and their corresponding thicknesses are shown in Figure 2.14. The specimen made of Al with wall thickness of 1.2 mm was scanned using an XRADIA XRM 410 system with a tungsten target at four different magnifications resulting in datasets with 4.8 µm, 7 µm, 14 µm and 21 µm voxel sizes. The first three datasets were used in *Paper III* and the last three were used in *Paper IV*. A 4 by 4 mm region at the center of each specimen at the same height in Al and Ti specimens was scanned using 4.8 µm
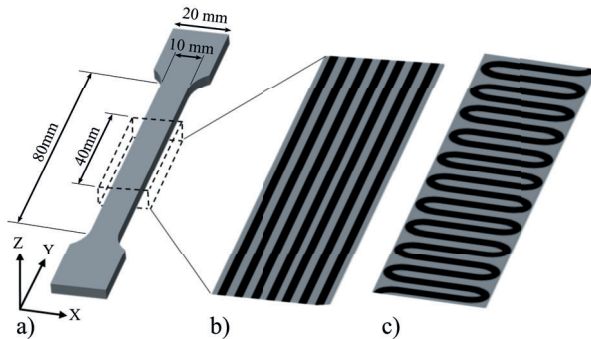

Figure 2.13: a) CAD design and orientation of the specimens used in Paper II. The dashed box shows the CT scanned region and schematic of b) longitudinal and c) transverse infill filaments.
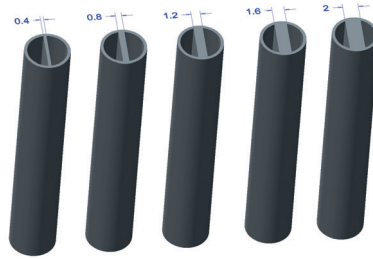
Figure 2.14: CAD design and dimensions of the specimens in mm.

voxel size which was used for surface characterization analysis performed in *Paper VI*. 80 kV, 125 µA and 1600 projections were used for this scan. The analyses, including the surface determination and other measurements, were performed using the commercially available software VGStudio MAX 3.0.

In *Paper VI*, the following method was used for measuring the 3D volume parameters (Vmp, Vmc, Vvc, and Vvv). Initially, the surface region, which is defined as the region between the highest peak and deepest valley of the surface, was selected in each specimen. The surface region was then divided into 1 µm thick slices, where the normal of all the slices is parallel to the normal of the surface. Using VGStudio MAX 3.0, the area of each slice was calculated and used for generating the areal material ratio curve of each specimen's surface region. The 3D volume parameters (Vmp, Vmc, Vvc, and Vvv) described in the ISO 25178-2:2012 were calculated from the areal material ratio with the help of an in-house generated MATLAB code. A schematic illustration of a surface region and how surface features and the 3D volume parameters correspond to the material ratio curve are shown in Figure 2.16.

As mentioned previously, the surface-based periodic cellular structures are manufactured for lightweight applications. The designed thickness of the walls used in these structures may vary between 400 to 4000 µm depending on the geometry and application. The geometrical deviation of as-designed versus as-built geometries due to the surface texture of the thin walls may affect the structural response of them, resulting in not fulfilling the strength requirement of the component. Varying the designed thickness of thin walls can potentially influence the microstructure, which may affect the mechanical strength. However, the details of microstructure study as well as a statistical approach for calculating surface region of specimens are not explained in this thesis and can be found in *Paper V*. In the studies performed in *Paper V*, six flat AlSi10Mg tensile specimens with thicknesses of 0.4, 0.5, 0.7, 1.0, 2.0 and 4.0 mm were manufactured. An EOS M290 Laser Powder Bed Fusion (LPBF) machine with built layer height thickness of 30 µm was used for this purpose. The design and dimensions of the specimens and their build direction are shown in Figure
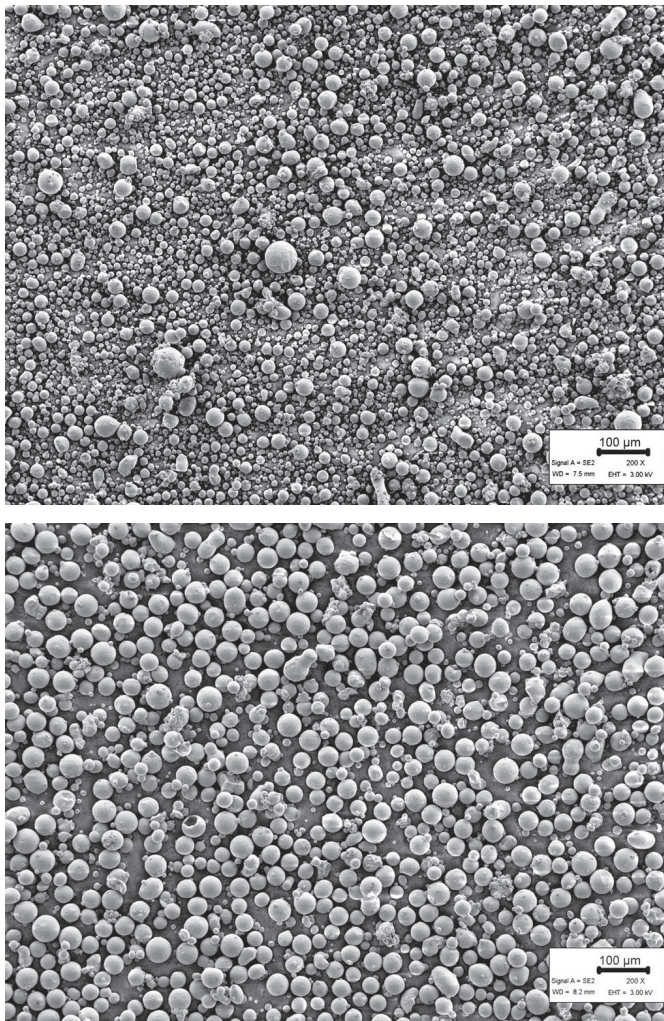
Figure 2.15: Powder particle size distributions of AlSi10Mg (top) and Ti6Al4V (bottom).
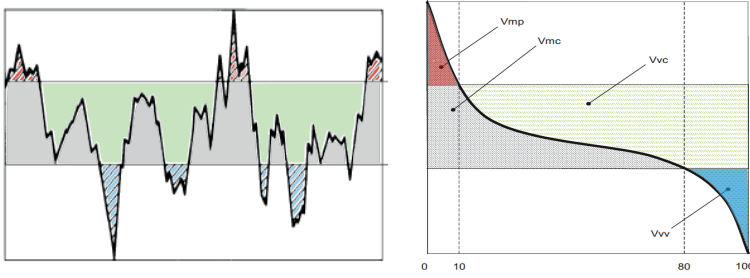
Figure 2.16: Schematic of surface region (left) and the corresponding material ratio curve and 3D volume parameters (right).

2.17. One set of the specimens were heat-treated according to the specification defined in [82]. Another set was used in as-built state without performing any post-processing. Uniaxial tensile tests were conducted at ambient room temperature using an MTS Sintech 20D with a 100 kN load cell in accordance with ISO 6892-1: 2016 [84]. The thicknesses of specimens were initially measured using micrometer in order to be used for a more accurate calculation of the tensile strength of them. Several measurements were performed at the gauge length of each specimen, and the mean values of width and thickness were recorded. CT analysis using a Bruker Skyscan 1272 was performed on a section of each specimen from both as-built and heat-treated sets. The CT parameters used for the CT scans were not identical for all the specimens since the thickness of the
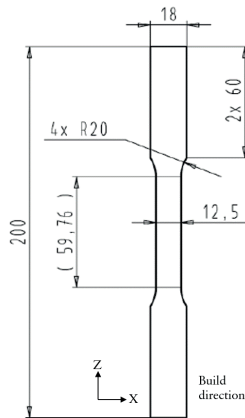
Figure 2.17: CAD design and dimensions (in mm) of the specimens used in Paper V.

scanned samples were not the same. However, all the specimens were scanned using the same voxel size. A section from each dataset was used for further surface and defect analysis using VGStudio Max3. The defect analysis was performed on the scanned samples in order to account for the potential effects of defects on the strength of the thin wall structures.

Chapter 3
Results of using CT in AM

In this chapter, the results of using CT for assessment of AM components are presented. The chapter starts with a general overview of using CT for dimensional measurements and follows with other applications such as strength evaluation and surface roughness investigation. In each section, there are discussions regarding how CT, in combination with other experiments, has resulted in information for the development of AM components or better design of them. The following subsections of this chapter mainly present CT analysis performed on internal geometry, porosity, and surface roughness, which have been used in the publications of this thesis.

3.1   CT for Dimensional Measurements

In this thesis work, CT has been used as an inspection tool for investigation of AM parts mainly for assessment of micro-scale internal features and AM surfaces. However, CT can be used for the geometrical inspection, and dimensional measurement of an AM part. Comparison of the CAD design and the as-built geometry of an AlSi10Mg AM part, as shown in Figure 3.1 a, is an example of geometrical inspection. The result of actual to nominal comparison of the component is illustrated in Figure 3.1 c. The relatively high geometrical deviation due to residual stresses at the free ends of the component is clear at the free end of the component. Also, the micro-scale deviations due to the rough surface are visible in the figure. Due to insufficient CT resolution for investigating AM surfaces in this dataset, further in-depth analysis on the dependency of AM surfaces on the design thickness of thin-wall structures is presented in chapter 3.4.

3.1.1   Dimensional Assessment of Internal Features

The result of CMM measurement performed on the external features of the test sample showed some deviation from the CAD design measurements. The
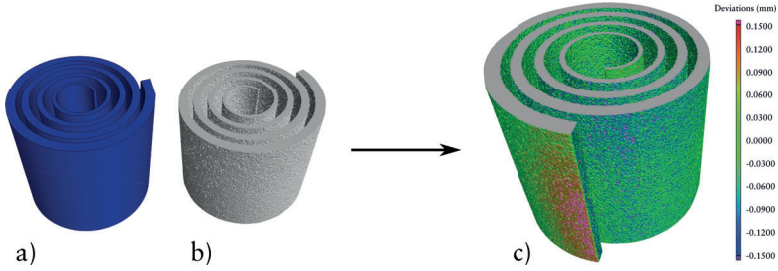
Figure 3.1: a) CAD design of an AM component b) Reconstructed 3D volume obtained from CT and c) The geometrical deviations due to residual stresses and the surface roughness.

distance measurements between the external half-spheres showed reasonably low (less than 1%) deviation from the CAD data. However, the measurement of diameters showed larger deviations, which were increased by decreasing the designed diameters of the half-sphere. The deviation of CMM diameter measurements form the CAD values for D1, D2, and D3 were 2.2, 3, and 10% respectively. This shows the effect of surface roughness, which impacts the diameter measurements, but it has a minor impact on the center to center measurements.

The deviation between the results obtained from the calibrated CT data and the CMM was in nearly the same range as the deviations between the results obtained from CAD and the CMM. This means that the CT measurements were in good agreement with the CAD designed measurements. However, this was not true for the features with diameters equal and less than 1mm. The reason is that the capability of the LPBF method for accurately generating those features drops significantly due to the surface roughness. The 4%, 13% and 39% CT versus CAD deviation of DI4, DI5, and DI6 respectively confirms this finding. A very low deviation between CT and CAD for the center to center measurements, on the other hand, the method is well capable of generating the features in the designed place accurately. The results of this study are valid for this test sample with the mentioned geometry, material, and the build orientation.

3.2   CT for Strength Evaluation of AM Components

In the following subsections, the CT is mainly used for assessing the mesoscale geometrical features of AM components to reflect their impact on the strength performance of them under mechanical loads.

Table 3.1: Uniaxial tensile test results of FDM specimens.

Fabrication temperature (°C)	Tensile strength (MPa)	Young's modulus (GPa)	Strain at break (%)
180	25.77±0.5	2.25±0.0	3.06±0.0
190	24.29±0.7	2.21±0.1	3.07±0.5
200	29.93±1.7	2.75±0.1	3.56±0.4
210	31.74±1.0	2.77±0.1	3.23±1.1
220	33.49±0.7	2.95±0.1	2.93±0.3
230	34.15±1.3	2.81±0.1	2.89±0.4
240	34.69±0.4	2.86±0.0	2.40±0.4
250	37.38±0.4	2.93±0.1	2.33±0.1
260	37.79±2.0	3.05±0.1	2.20±0.1

3.2.1 Mechanical Strength of FDM Components

This section presents the results obtained in ***Paper II*** which deals with the application of CT for investigating the mechanical strength of parts manufactured using FDM. The design, material, and experimental work were explained in chapter 2.5. The main interest for investigating the internal geometry of the FDM specimens was to correlate the mechanical strength of the parts with their internal geometry, which was caused by the manufacturing process. The result of the uniaxial tensile test showed the temperature dependence of the tensile strength as is presented in Table 3.1. The Young's modulus and percentage of elongations were also affected by the fabrication temperature.

Using CT, the total volume of the specimens and consequently, the weight of them were obtained. The results of weight measurements using CT data showed the same trend as compared with the data obtained from the scale. A considerably poor external dimensional accuracy was observed in as-built geometry of specimens fabricated at a lower range of fabrication temperatures, such as 180 °C and 190 °C. Figure 3.2 a, b, and c show the CT reconstructed geometry of specimens at scanned regions fabricated at 180, 220 and 260 °C respectively, in which the difference in quality of prints depending on the fabrication temperature is shown.

The same phenomenon could be observed by looking at the internal geometry of specimens. Figures 3.3 and 3.4 show the quality of the bond between filaments as well as air gaps. In the specimens fabricated at the lower temperatures, bigger airgaps were observed due to improper deposition of the filaments, which confirms the weight measurement results. The extruded filaments bonds are weaker for the specimens fabricated at lower the temperatures. However, increasing the fabrication temperature improves the bond by and considerably decreases the airgaps.

The porosity analysis showed that fabrication temperature highly influences the porosity in FDM parts. It was observed that the porosity increases linearly by decreasing the fabrication temperature in a way that an increase in the fabrication temperature from 180 °C to 260 °C decreases the porosity by six times. The results also showed that no considerable change in porosity occurs for the fabrication temperature above 240 °C.

In order to consider the effects of the internal geometry of the specimens on their mechanical strength, the strength values were recalculated based on porosity (weight). The new strength values (specific strength) experienced improvement compared to the values obtained directly from the tensile test. However, the porosity could not fully explain the discrepancy of the obtained strength results. Therefore, a more in-depth approach by selecting minimum cross-sectional areas with the help of the CT data was used for recalculation of the ultimate tensile strength results. The area of minimum cross-sections was selected at regions with highest local porosity, which in fact are the regions where the local stresses are maximum. The strength recalculation showed a considerable improvement compared to the recalculation performed using the porosity as is presented in Figure 3.5. This means that porosity is not necessarily the only parameter affecting the strength, and the specimens were experiencing relatively high local stresses due to their internal geometry.

The CT investigations provided further information which helped to explain the other differences in the mechanical strength of the FDM parts, for example, the higher percentage elongation and lower Young's modulus of the specimens fabricated at the lower temperatures. Firstly, significantly smaller width of transverse extruded filaments deposited at the lower temperatures due to inconsistent deposition resulted in lack of fusion and consequently lower mechanical strength. Secondly, the bonds at turns were weak, especially with the adjacent turns and the contour filaments (walls), causing the specimens to act as a spring thus considerably higher percentage elongation and lower Young's modulus.
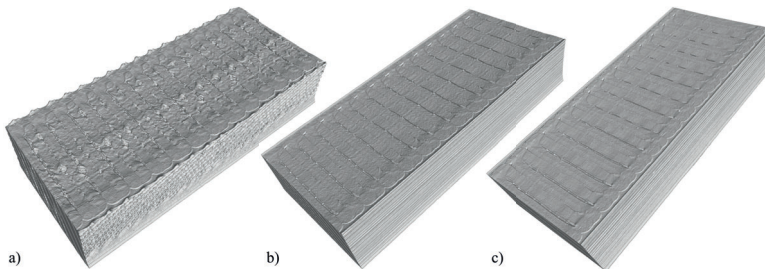

Figure 3.2: CT reconstructed geometry of scanned regions for specimens fabricated at a) 180 °C, b) 220 °C, c) 260 °C.
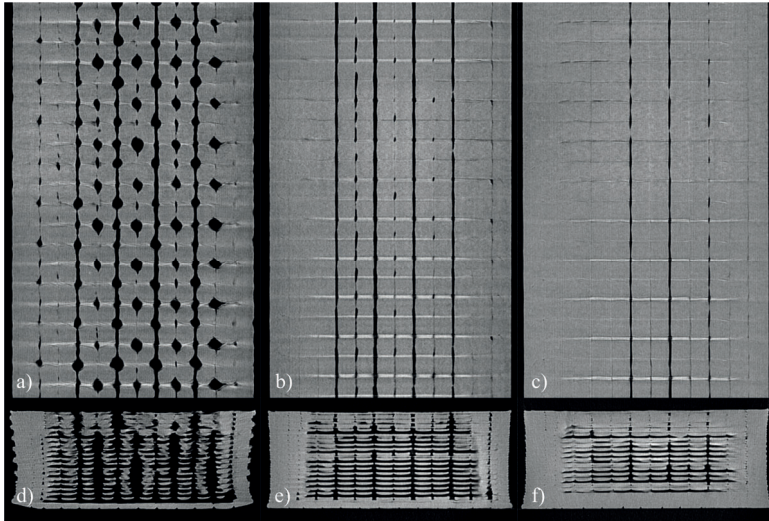
Figure 3.3: Cross-sectional areas of specimens fabricated at 180 °C, 220 °C and 260 °C at a), b) and c) XY plane and d), e) and f) XZ plane.

Finally, the inhomogeneous deposition resulting in various local density in each specimen regardless of the fabrication temperature shows that 100% infill is not reachable as a result of this manufacturing process. Therefore, further research and development are required to improve the quality of deposition to achieve the desired mechanical properties. The application of controlled local density by varying, for example, nozzle temperature or travel speed, on the other hand, can open up the possibility of manufacturing parts with tailored local strengths or controlled anisotropy.

Figure 3.4: Bond quality of transverse filaments for specimens fabricated at a)180 °C to i)260 °C respectively (top XY plane and bottom YZ plane).
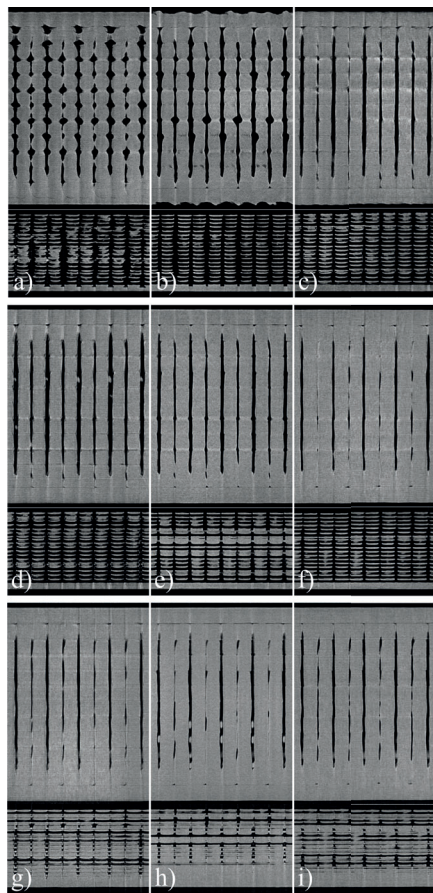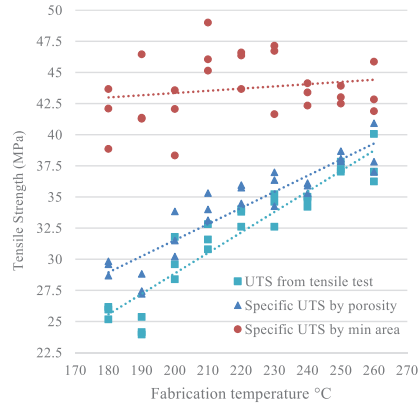
Figure 3.5: Specific strength values calculated based on CT results.

3.2.2 Mechanical Strength of LPBF Thin Walls

This section mainly presents the results obtained in *Paper V* in which the thickness dependency of AlSi10Mg thin wall structures was investigated. Initially, the micrometer thickness measurement results showed that all the measured thicknesses were larger than as-designed. It was also clear that the deviation between as-built and CAD designs significantly increases by decreasing the designed thickness of the specimens. For example, the 0.4 mm thick specimens were on average 60% thicker than the intended CAD designed 0.4 mm while the specimens designed to be 4.0 mm were on average only 3.4% thicker than their CAD designed thickness. The deviation for 0.5, 0.7, 1.0, and 2.0 mm specimens were respectively on average 39.2, 29.6, 19, and 7.3%, which shows a considerable decrease.

The results of the uniaxial tensile test showing the UTS of both as-built and heat-treated specimens is presented in Figure 3.6. The results are based on the measured area obtained from micrometer measurements, which show a remarkable thickness dependency. While the specimens with the thicknesses of 2mm and 4 mm show nearly the same UTS, the thinner specimens had significantly lower tensile strengths. A significant difference between the obtained values of this study and the material's specifications, claimed by the manufacturer. The microstructure analysis did not show any considerable effect of thickness variation. For example, all the as-built specimens had hardness values around 125 HV, and all the heat-treated specimens had a hardness of around 80 HV. Therefore, it was assumed that microstructure could not be the cause of lower UTS of the thinner specimens and further investigation on internal defects and surface morphology was done with the help of CT.
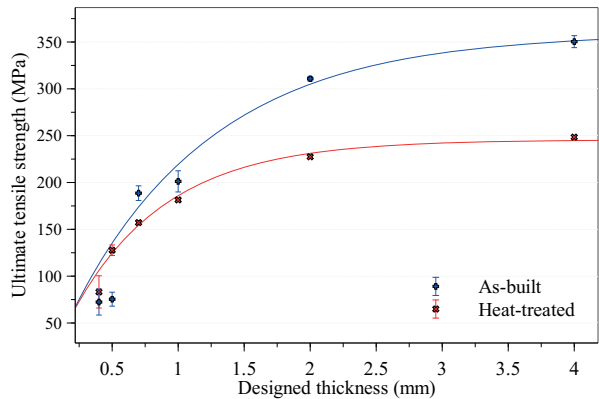
Figure 3.6: Ultimate Tensile Strength of the specimens.

The results of surface morphology analysis using CT provided detailed information about the surface region of specimens. The maximum and minimum thickness of each specimen by measuring the distance between the highest peaks and lowest valleys at the scanned region revealed a more accurate load bearing area of each specimen. The results of CT thickness measurements are provided in Figure 3.7 in which the error bars show the absolute maximum and minimum measured thickness. As it is shown, the maximum thickness measurements results are in good agreement with the results obtained from the micrometer measurement. The small difference in the obtained values from the

Figure 3.7: CT results of maximum and minimum thicknesses measurements.

two different methods can be the result of a relatively larger measured area when the micrometer is used.

Another important finding is that the average thickness of all the specimens regardless of their designed thickness has a negative deviation between 10 to 15% from their corresponding designed thicknesses. Finally, the most critical finding using CT is the negative thickness deviations, wh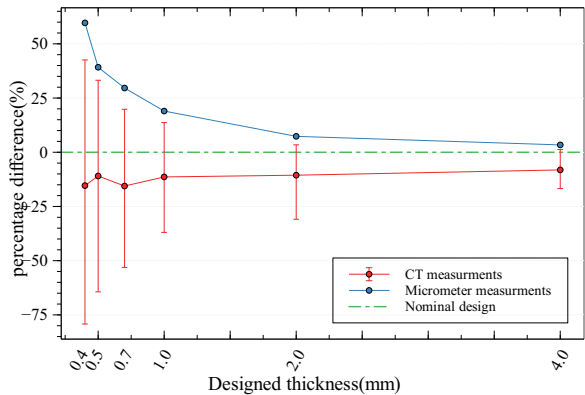ich are highly influenced by the changing of the designed thickness. As the designed thickness decreases, the measured absolute minimum thickness significantly increases so that for the 0.4 mm specimen 79% negative deviation was observed. This means that in 0.4 mm specimens there are regions at which the thickness is around 80 μm while for the 4.0 mm specimen the smallest thickness was around 3500 μm. The results of thickness measurement using CT proved that the geometrical inaccuracy of the specimens mainly due to the surface morphology which can be resolved only with the help of CT could be potentially the reason for the discrepancy of tensile strength results. Therefore, using the average thickness values, the new load-bearing area of each sample was calculated and used for recalculation of the tensile test results, as shown in Figure 3.8. The newly obtained results show an increase in UTS values. However, the UTS values of specimens with thicknesses less than 2 mm does not obtain the UTS expected form this material.
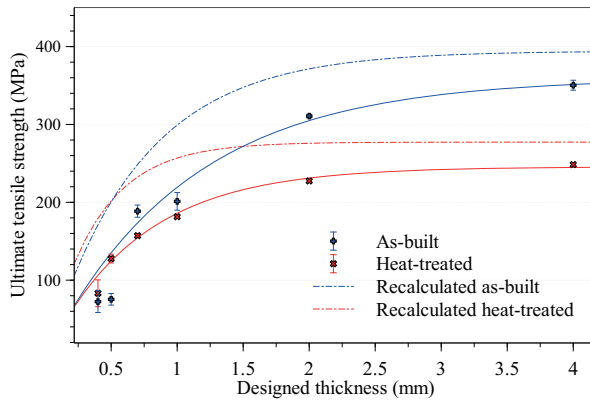
Figure 3.8: Updated graph of tensile test recalculated with the average thicknesses of the corresponding specimen obtained from CT.

In order to explain the differences in the recalculated UTS values, the internal defects of the samples were also investigated for their potential effect on the mechanical strength. The results of the porosity analysis are provided in Figure 3.9. The defect analysis in the scanned regions showed that the porosity does not change with a thickness variation of the specimens. All the specimens on average, had around 99.98% material content. It was also observed that the av-

erage diameter of the ten largest pores in all specimens is in range of 60 to 100 μm. The largest pores of the thicker specimens were relatively larger than those of thinner specimens which can be explained by their larger scanned volumes. The sphericity of pores was higher in the thinner samples, and a considerable number of large pores was observed at the subsurface of the thicker specimens.

Figure 3.9: The diameter of the 10 largest pores and porosity obtained from CT.

From the obtained results, it can be concluded that the porosity cannot be the influential parameter affecting the strength results. However, considering the very small thickness of thinner specimens at some sections and the size range of the large pores, it can be concluded that high local stress concentration as 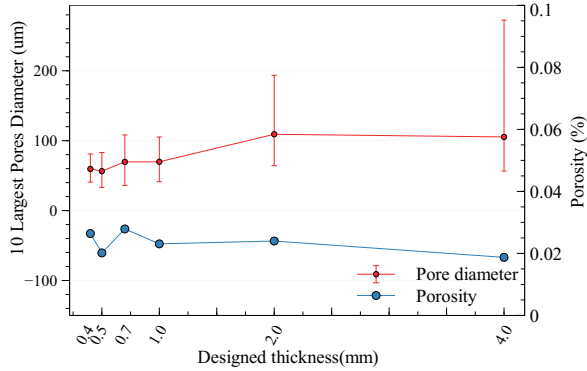a result of deep valleys at surface and porosity have led to premature failure of specimens with a thickness of 1 mm and below.

3.3 Effects of CT Magnification

This section mainly focuses on the effect of CT magnification as one of the influential CT parameters, on the measurements obtained from CT data. The results of magnification variation on the surface morphology and porosity of an Al10SiMg test sample which is provided in *Paper III* and *IV* respectively are presented here. The main motivation of investigating such a parameter comes from the industrial need for non-destructive inspection of large components for quality assurance. The size of components becomes a limiting issue for inspection of parts using higher resolutions. Therefore, it is crucial to know how and up to which extent the magnification and consequently, the achieved resolution could affect the analysis results. The specimen with 1.2 mm wall thickness shown in Figure 2.14 was CT scanned at three different magnifications, and the result was datasets with 7, 14 and 21 μm voxel sizes. All the other CT parameters, including the data acquisition settings and segmentation (ISO 50)

were identical except the voxel size in order to investigate only the effect of magnification.

The qualitative comparison of surface features from the three different datasets is shown in Figure 3.10. As it is illustrated, the voxel size has a significant influence on the obtained surface texture of reconstructed volumes. The volume made of larger voxel size lacks the surface feature details, for example, the partially attached powder particles which can be observed in the volume with smaller voxel size. A better illustration of how a peak or a deep indent would be segmented in different volumes is illustrated in Figure 3.11.
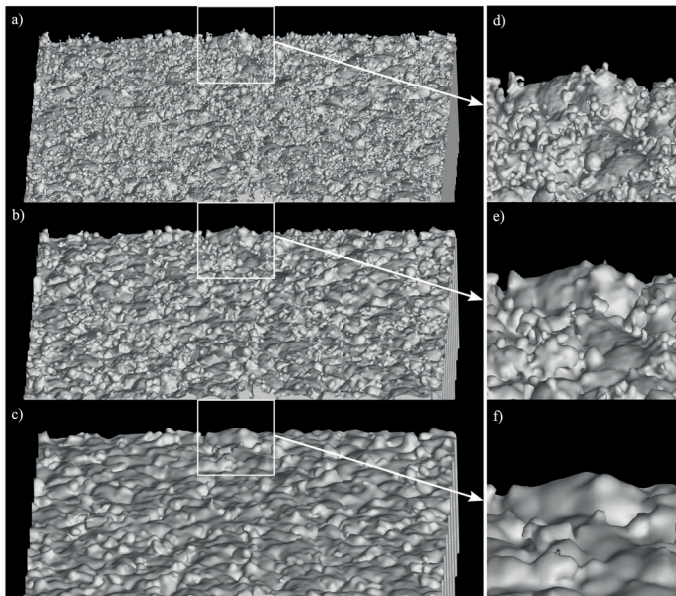
Figure 3.10: a), b) and c) 3D reconstructed CT volumes, displaying the surface of the specimen obtained from the dataset with voxel sizes of 7, 14, and 21 m respectively d), e) and f) A selected region showing more details from the dataset with voxel sizes of 7, 14, and 21 μm respectively.

The quantitative results of comparing the height and depth of the 20 highest peaks and the 20 deepest valleys as a percentage of the surface region thickness (presented in Figure 3.12 and Figure 3.13) show that the measurements are highly dependant on the CT magnification. Considering the high magnification data set as the ground truth, the medium and low magnification datasets measure equal or smaller values for peak measurements. In addition, the values obtained from the medium magnification scan, are between the measured values from high and low magnification data sets for both peak and valley
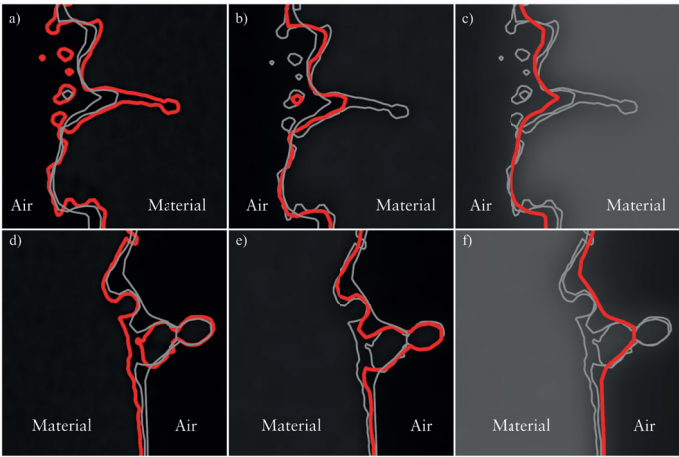
Figure 3.11: a), b), and c) A selected valley and resulting ISO surfaces obtained at high, medium and low magnifications respectively. d), e) and f) A selected peak and resulting ISO surfaces obtained at high, medium and low magnifications respectively.
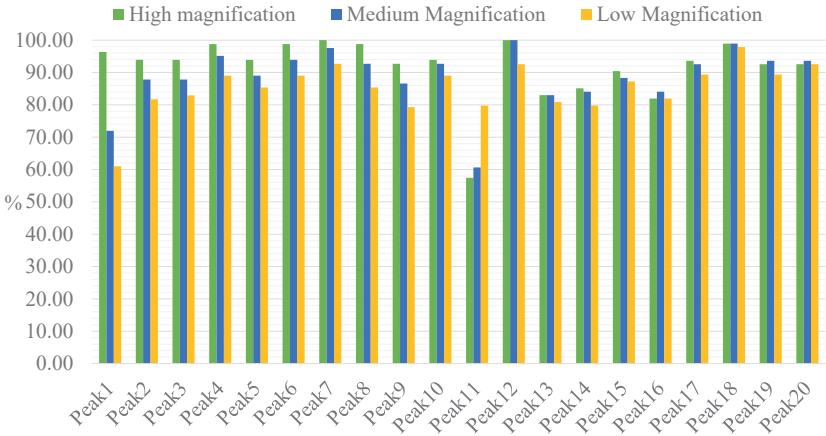
Figure 3.12: Measurement of peaks heights as the percentage of surface region thickness.
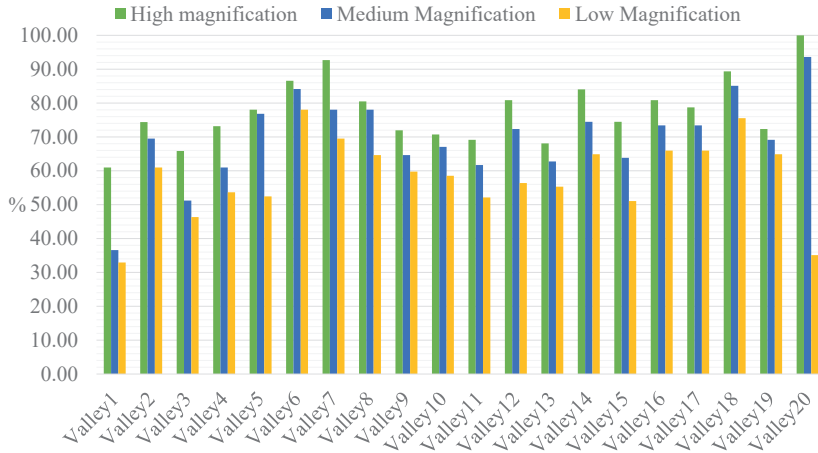
Figure 3.13: Measurement of valleys depths as the percentage of surface region thickness.

measurements. However, the values at some valleys were closer to the values of high magnification, and in other valleys, they were closer to the values of low magnification. The values obtained from medium and low magnification data sets underestimate the depth of valleys compared to values obtained from the high magnification data set. A relatively larger deviation in values of valley measurements can be observed compared to peak measurement. Meaning that the difference in peak measurements even between low and high magnification data sets was nearly the same while the values of valley measurements obtained from low magnification data set were considerably lower than high magnification values.

The maximum and minimum thicknesses of the AM thin-walled specimen, which respectively are the result of the peak to peak and valley to valley measurements, showed a noticeable dependency on CT magnification. The maximum thickness value for medium and low magnification data sets were underestimated by 0.5% and 2% respectively. The minimum thickness values, on the other hand, overestimated even at a more considerable level by measuring 8.5% and 18.5% more than the measured value obtained from the high magnification data set. This means that the lower magnification scan underestimates both peak and valley measurements and depth of valleys and re-entrant features were underestimated at a more considerable level compared to the measurement of peaks.

A similar phenomenon was observed after investigating the effects of CT magnification on porosity measurements. Figure 3.14 shows the result of poros-
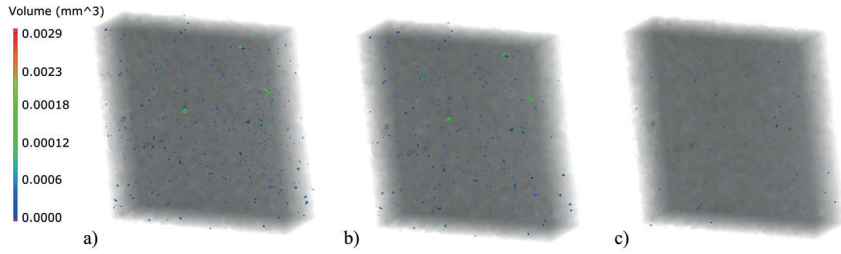
Figure 3.14: Porosity obtained from the datasets with voxel size: a) 4.8 μm b) 7 μm and c) 14 μm.
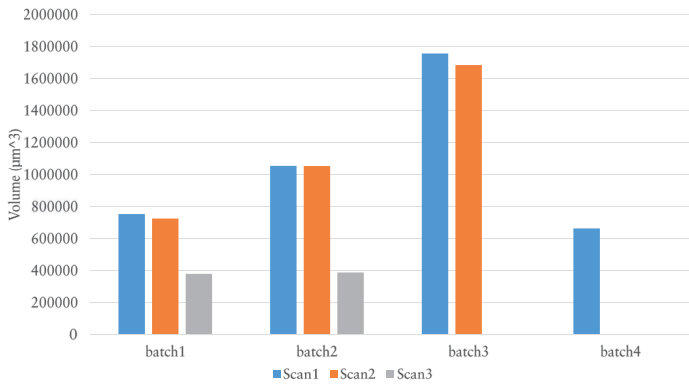
Figure 3.15: Total volume of pores in each batch detected using different scans.

ity analysis performed on the same volume using scan1, scan2, and scan3 with respective voxel sizes of 4.8, 7, and 14 μm. Both the quality and quantity of the measurement were influenced by the magnification. The number of resolved pores in datasets obtained from scan1, scan2 and scan3 were 579, 229 and 28 respectively with 0.0230%, 0.0188% and 0.0041% porosity. In order to compare the results of different scans, the pores were categorized (based on their volumes) in 4 batches. The five largest pores of scan one (reference scan) were put in batch 1 (Large), the next 22 pores were put in batch2 (medium), the next 200 were put in batch 3 (small) and the rest in batch 4 (very small). The total volume of each batch obtained from scan1, 2, and 3 are presented in Figure 3.15.

As it is shown in Figure 3.15, the measured volume of the pores in batch one obtained from scan 1 and 2 are nearly the same while it is almost twice the value obtained from scan3. The sum of the volume of pores in batch two

Table 3.2: 3D volume parameters (µm) at p 10% and q 80%.

		0.4	0.8	1.2	1.6	2.0
	Vmp	2.92	2.5	1.96	2.43	2.55
Al	Vmc	36.15	37.15	26.82	33.01	27.28
	Vvc	69.42	65.43	43.89	56.61	50.39
	Vvv	3.04	4.46	4.02	5.01	4.03
	Vmp	1.94	1.85	2.02	1.77	1.68
Ti	Vmc	25.39	28.51	24.20	24.08	25.94
	Vvc	51.29	56.14	48.50	46.63	45.76
	Vvv	1.33	1.74	1.61	1.56	1.64

obtained from scan3 is around 30% of the values obtained from scan1 and 2. A similar pattern of nearly the same volume measurements in pores of batch3 obtained from scan1 and 2 can be observed while the scan3 fails to resolve the pores in this batch. Finally, the volume of pores in the batch four could be measured only using the data of scan1, and both scan2 and 3 were unable to detect any pore. The main difference between the porosity results of scan one and two was observed in batch4.

The CT magnification not only affects the porosity results and the pore counts but also the morphological information of the pores. The morphological analysis of the largest pore showed that the sphericity obtained from scan one, two and three were 0.4, 0.46, and 0.6, respectively, which means that the lowest magnification scan smooths out the morphology of the pore and provides false information.

3.4   CT for Surface Roughness Determination

The in-depth surface roughness analysis of AlSi10Mg (Al) and Ti6Al4V (Ti) thin-wall structures are presented in this section. The CT results obtained in *Paper VI* revealed that the surface region in the Al specimens is larger than those of corresponding specimens in the Ti batch. The qualitative observation of the surfaces obtained from the CT showed that the accumulation of partially melted powder particle could be the reason for this phenomenon. Considerably larger surface regions for Al specimens compared to their corresponding specimen in the Ti was obtained after plotting the material ratio curves of the specimens as presented in Figure 3.16. For a better comparison, the material ratio curves are overlapped at the plane with the 50% aerial material ratio. Comparing the Vmp and Vvv 3D volume parameters for Al and Ti specimens as presented in Table 3.2 shows that all the Al specimens (except Al1.2) have larger peak volumes as compared to their corresponding specimen in Ti batch. The volume of valleys in all of the Al specimens was larger than their corresponding volume of valleys in the Ti batch.

Looking at Figure 3.16 a, a very similar transition from 30% to 80% areal material ratio can be observed for the 0.4 mm and 2.0 mm Al specimens. However, the peak volume of 0.4 mm Al specimen is relatively larger than that of 2.0 mm Al specimen. This is the opposite though for the valley volume of these two specimens. In addition, the peak volume of 0.4 mm Al specimen is at a further distance from the 50% aerial material ratio plane as compared to the 2.0 mm Al specimen. For the valleys, the 2.0 mm Al specimen valley volumes are at a further distance from the 50% aerial material ratio plane as compared to the 0.4 mm Al specimen. No specific transition in the material ratio curves of rest of Al specimens (Al 0.8, Al 1.2 and Al 2.0) was observed. However, the 0.4 mm and the 0.8 mm specimens had the largest peak volumes among the other, and the thickest and the thicker specimens showed relatively larger valley volumes. The same phenomenon of having large peak volume for thinner specimens and large valley volume for thicker specimens with less intensity can be observed for Ti specimen as it is shown in graph Figure 3.16 b. All the Ti specimens showed very similar material ratio curves with nearly the same surface region thickness providing better dimensional accuracy for Ti specimens as compared to Al specimens.

Based on Figure 3.16 c, the peak height and peak volume of Al specimen are considerably larger than that of Ti comparing the thinnest specimens of Al and Ti. The volume of valleys is significantly larger for 0.4 mm Al specimen as compared to 0.4 mm Ti. The depth of valleys for Al specimen is at a further distance from the 50% material ratio. Comparing the two thickest specimens of different materials, as shown in Figure 3.16 d, the difference in volumes of the peaks is very low. However, the volume of valleys for 2.0 mm Al specimen though is still significantly larger than 0.4 mm Ti, which is due to numerous close to surface re-entrant features. The results of 3D volume parameters derived from the material ratio curves, which are presented in Table 3.2 confirm the above-explained discussions.

Based on the application of the surface analysis, other values of "p" and "q" instead of (p10%) and (q80%) can be used. For example, depending on the desired mechanical response of a surface-based cellular structure, the information of a larger volume of peak or valley is required. Therefore, the volume parameters at p 30% and q 70% are calculated and presented in Table 3.3, which can be useful for better design of surface-based cellular structures.

The larger peak volumes in both Ti and Al thinner specimens, which is mainly due to the attachment of partially melted particles can be explained as the result of various phenomena. Firstly, it should be considered that the primary heat dissipation in LPBF method occurs by conduction to the build plate through the part itself. The smaller cross-sectional area of the thinner specimens as compared to the thicker specimens may change the heat conduction scenario. It is assumed that the conduction in the thinner specimens becomes two-dimensional while for thicker specimens due to the larger volume of material remains three dimensional. This can result in a heat accumulation state
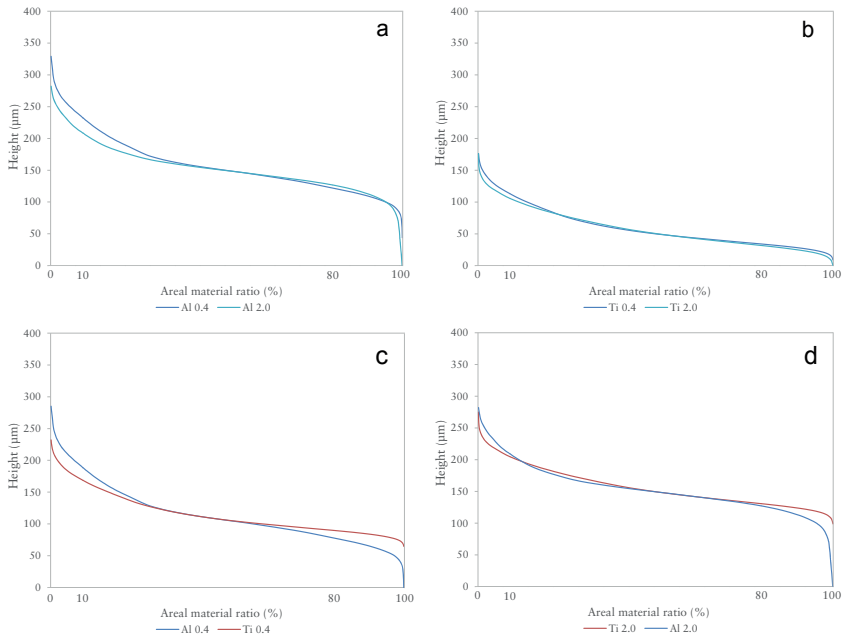
Figure 3.16: Comparison of material ratio curves overlapped at 50% areal material ratio, a) Al0.4 and Al2.0; b) Ti0.4 and Ti2.0; c) Al0.4 and Ti0.4 and d) Ti2.0 and Al2.0.

Table 3.3: 3D volume parameters (µm) at p p 30% and q 70%.

		0.4	0.8	1.2	1.6	2.0
	Vmp	13.73	11.84	8.09	10.67	9.81
Al	Vmc	17.19	18.88	13.94	16.55	14.09
	Vvc	18.67	19.96	13.94	17.30	14.78
	Vvv	5.84	7.48	6.24	7.74	6.06
	Vmp	9.73	10.09	9.09	8.80	7.83
Ti	Vmc	13.86	15.86	13.47	13.37	15.36
	Vvc	16.01	19.00	15.42	15.51	17.51
	Vvv	2.58	3.30	2.93	2.86	3.18

in the thinner specimens, which provides enough energy for locally melting the surrounding powder particles. The spherical morphology of these attached particles confirms this hypothesis. Also, the possible difference in the energy density or scanning speed of laser for scanning a contour or the infill may also be the reason for this issue. Since all the process parameters except the layer height were unknown for this study, more information is needed for concluding this hypothesis.

The proposed method in this thesis for investigating the AM surface provided valuable information on the surface, which is essential for mechanical strength prediction of thin-wall components such as surface-based cellular structures. The combination of material ratio curves and the 3D volume parameters do not only present the height of the surface region and its transition. The volumetric information of the peaks (Vmp), as well as its distance from a reference plane in the surface region (for example, 50% aerial material ratio), provides the information about the portion of the surface which has less contribution to the mechanical strength. The same information can be obtained from (Vvv) where the magnitude of this parameter as well as the depth of valleys can help to estimate the mechanical response better.

Chapter 4
Summary

4.1 Concluding Remarks

In this thesis, CT has been used for quality assessment of components manufactured using AM. Despite all the capabilities of AM and the possibilities that AM methods have brought, undesired imperfections associated with the processes of fabrication were observed in AM components. Porosity of components is one of the limiting phenomena affecting the mechanical performance of AM components. The mechanical strength of parts manufactured using FDM has dependency on the porosity which was the result of the fabrication process. Porosity was found in the LPBF manufactured metallic thin-walls that are the constituting component of surface-based periodic cellular structures. The porosity in combination with the complex surface texture, the other limiting phenomenon in the powder bed AM methods, had a considerable influence on the mechanical performance of thin-wall structures. It was concluded that the dimensional deviation between as-built and as-designed wall thicknesses will be affected, depending on the designed thickness and the application of two commonly available powder materials. Thus, the variation in design (thickness) affects the as-built quality and consequently the mechanical response of these structures. As the conclusion, the design of AM lightweight structures, with the help of surface-based periodic cells, requires consideration of the mentioned mesoscale surface-related imperfections.

AM is a relatively new method and needs yet further research and developments. These developments need to be performed differently in many aspects. One cannot use the traditional CAD design systems since they are designed based on the available manufacturing method of that time. In addition, the limitations and the challenges of AM are not considered in such design systems. This issue is also valid for the tools that should be used for the evaluation of components manufactured with AM. The traditional evaluation methods cannot be used for a thorough investigation of periodic cellular structures or the surface texture of AM parts. Likewise, the same tools cannot be used for an

in-depth characterization of AM surfaces. The traditional surface parameters which are defined based on the requirements and limitations of the manufacturing methods back in time, cannot fully reflect the complexity of AM surfaces. The new surface complexity of AM requires a different way of looking at the problem and defining or using parameters which are capable of addressing and presenting these limitations in more informative ways.

The results of these studies have shown that CT has high capabilities for providing useful and reliable geometrical information of AM components, which cannot be obtained using other inspection methods. Concerning the CT data, a general conclusion is that the "quality of the CT data" is the crucial factor that has significant impact on the accuracy of the results, regardless of the parameter setting and the procedure used. Obtaining decent CT datasets is the crucial step for using CT as a a measurement tool, while the lack of standard procedures for data acquisition is still a challenge.

Regarding the AM surfaces, appropriate inspection tool, the right post-processing analysis and right representing methods should be used. The proposed method in this thesis for investigating the AM surface has shown to be capable of providing valuable information of the AM surfaces, when the mechanical strength of surface-based cellular structures is of concern. Moreover, the mentioned information has to be considered in the design stage of cellular structures so that a more accurate mechanical response of cellular structures be estimated.

4.2 Future perspective

The future outlook in both fields of CT and AM seems promising. However, the high cost of using AM for the fabrication of components may remain a challenge. With the help of developed in-situ monitoring systems on the one hand and more advanced numerical simulations, on the other hand, the process parameter of the AM methods can be more accurately optimized. More advanced AM design tools may need to be developed, such as CAD software packages that are designed to account for the limitation of AM methods. The effects of support structure, heat dissipation, residual stresses, microstructure, and consequently, the part quality and mechanical performance, can be optimized using these tools.

Regarding the periodic cellular structures, in-situ mechanical tests, performed in combination with high resolution CT, will provide more information about the failure mechanism of these structures. Using the iterative reconstruction methods and digital volume correlation (DVC) to perform fast scans for capturing the failure process (4D CT scanning) would provide even more detailed knowledge about the mechanical performance of cellular structures. Modern CT systems that use phase contrast method are capable of providing 3D crystallographic information of the sample to be scanned. These systems can con-

tribute even more for a better investigation on the cellular structures' mechanical strength.

With the rapid improvement in the field of CT, especially in the hardware, a significant increase in the quality and reliability of the CT results is going to be achieved. This increase is expected to happen by eliminating some of the error sources. Two examples of advancements in the hardware development of CT field are the emergence of the new photon-counting detectors and the modern liquid-metal-jet tubes (which currently are available in customized-built systems and not the laboratory systems). The modern detectors, which have multiple channels for simultaneous capturing of low and high energy projections, can highly eliminate the challenges associated with the scanning of multi-material parts. The improvements on the software side is another path to be taken, especially the development of algorithms for minimizing CT artifacts.

A very currently non-realistic future perspective of using CT as a measurement tool is to benefit from concepts such as "internet of things" (IOT). Various CT scan results with different combinations of parameter settings, materials, etc. can be stored in a comprehensive platform of CT data bank. With the help of machine-learning algorithms, these data can be analyzed, and the patterns of CT parameters' effect can be thoroughly understood. These new solutions can eventually reduce the effect of errors or uncertainties in the CT results by minimizing the influences of human factors.

Finally, providing new CT standards, in which the expected requirements of the CT experts from different fields has been met, is essential for a more widespread and reliable applications of CT as a dimensional metrology tool.

References

[1] United Nations (Department of Economic and Social Affairs). World Population Prospects 2019: Highlights. Technical Report June, 2019. (Cited on page 1.)

[2] United Nations (Department of Economic and Social Affairs). The sustainable development goals report 2019. Technical report, 2019. (Cited on page 1.)

[3] European Environment Agency. National emissions reported to the UNFCCC and to the EU Greenhouse Gas Monitoring Mechanism. *National greenhouse gas inventories (IPCC Common Reporting Format sector classification)*, 2018. (Cited on page 1.)

[4] European Road Transport Research Advisory Council. ERTRAC Research and Innovation Roadmaps. Technical Report September, 2011. (Cited on page 2.)

[5] Giulia Fredi, Steffen Jeschke, Athmane Boulaoued, Joachim Wallenstein, Masoud Rashidi, Fang Liu, Ross Harnden, Dan Zenkert, Johan Hagberg, Goran Lindbergh, Patrik Johansson, Lorenzo Stievano, and Leif E Asp. Graphitic microstructure and performance of carbon fibre li-ion structural battery electrodes. *Multifunctional Materials*, 1(1):015003, aug 2018. (Cited on page 2.)

[6] Teknikföretagen. Made in Sweden 2030, Strategic Agenda for Innovation in Production. Technical report, 2013. (Cited on page 2.)

[7] Raoul Leering. 3D printing: A threat to global trade, 2017. (Cited on pages 3 and 7.)

[8] Iwan Zein, Dietmar W. Hutmacher, Kim Cheng Tan, and Swee Hin Teoh. Fused deposition modeling of novel scaffold architectures for tissue engineering applications. *Biomaterials*, 23(4):1169–1185, 2002. (Cited on pages 3 and 15.)

[9] Michele Bici, Salvatore Brischetto, Francesca Campana, Carlo Giovanni Ferro, Carlo Seclí, Sara Varetti, Paolo Maggiore, and Andrea Mazza. Development of a multifunctional panel for aerospace use through SLM additive manufacturing. *Procedia CIRP*, 67:215–220, 2018. (Cited on page 3.)

[10] Manish Kamal and Gregory Rizza. *Design for metal additive manufacturing for aerospace applications*. Elsevier Inc., 2019. (Cited on page 3.)

[11] Raquel Galante, Celio G. Figueiredo-Pina, and Ana Paula Serro. Additive manufacturing of ceramics for dental applications: A review. *Dental Materials*, 2019. (Cited on page 3.)

[12] ASTM International and ISO. ISO/ASTM 52900:2015 (ASTM F2792) Additive manufacturing , General principles , Terminology, 2017. (Cited on page 7.)

[13] Sara Biamino, Burghardt Kloden, Thomas Weibgarber, Bernd Kieback, and Ulf Ackelid. Titanium aluminides for automotive applications processed by electron beam melting. *Mpif*, 3:96–103, 2014. (Cited on page 7.)

[14] Huan Qi, Magdi Azer, and Prabhjot Singh. Adaptive toolpath deposition method for laser net shape manufacturing and repair of turbine compressor airfoils. *International Journal of Advanced Manufacturing Technology*, 48(1-4):121–131, 2010. (Cited on page 7.)

[15] Andreas Segerstark. *Additive Manufacturing using Alloy 718 Powder: Influence of Laser Metal Deposition Process Parameters on Microstructural Characteristics*. 2015. (Cited on page 8.)

[16] Jim Foster, Crawford Cullen, Stephen Fitzpatrick, Grant Payne, Liza Hall, and James Marashi. Remanufacture of hot forging tools and dies using laser metal deposition with powder and a hard-facing alloy Stellite 21®. *Journal of Remanufacturing*, 2018. (Cited on page 8.)

[17] Ajit Panesar, Meisam Abdi, Duncan Hickman, and Ian Ashcroft. Strategies for functionally graded lattice structures derived using topology optimisation for Additive Manufacturing. *Additive Manufacturing*, 19:81–94, 2018. (Cited on page 8.)

[18] A. O. Aremu, J. P.J. Brennan-Craddock, A. Panesar, I. A. Ashcroft, R. J.M. Hague, R. D. Wildman, and C. Tuck. A voxel-based method of constructing and skinning conformal and functionally graded lattice structures suitable for additive manufacturing. *Additive Manufacturing*, 13:1–13, 2017. (Cited on page 8.)

[19] Diab W Abueidda, Mohamed Elhebeary, Cheng-shen Andrew Shiang, Siyuan Pang, Rashid K Abu Al-rub, and Iwona M Jasiuk. Mechanical properties of 3D printed polymeric Gyroid cellular structures : Experimental and finite element study. *Materials & Design*, 165:107597, 2019. (Cited on page 8.)

[20] Oleg D Neikov. *Porous Powders and Metallic Foams*. Elsevier Ltd., 2 edition, 2019. (Cited on page 8.)

[21] John Banhart. Aluminum foams: On the road to real applications. *MRS Bulletin*, 28(4):290–295, 2003. (Cited on page 8.)

[22] John Banhart. Metal Foams, from Fundamental Research to Applications. *Frontiers in the Design of Materials*, pages 279–289, 2014. (Cited on page 8.)

[23] Hanna E. Burton, Neil M. Eisenstein, Bernard M. Lawless, Parastoo Jamshidi, Miren A. Segarra, Owen Addison, Duncan E.T. Shepherd, Moataz M. Attallah, Liam M. Grover, and Sophie C. Cox. The design of additively manufactured lattices to increase the functionality of medical implants. *Materials Science and Engineering C*, 94(March 2018):901–908, 2019. (Cited on page 8.)

[24] Lin Cheng, Jiaxi Bai, and Albert C. To. Functionally graded lattice structure topology optimization for the design of additive manufactured components with stress constraints. *Computer Methods in Applied Mechanics and Engineering*, 344:334–359, 2019. (Cited on page 8.)

[25] Michael F. Ashby. *Materials Selection in Mechanical Design*. Butterworth-Heinemann, fourth edition edition, 2011. (Cited on page 9.)

[26] Bintoa. Bits Into Atoms, 3D Printing & Design Co. (Cited on page 10.)

[27] Thomas Simson, Andreas Emmel, Anja Dwars, and Juliane Böhm. Residual stress measurements on AISI 316L samples manufactured by selective laser melting. *Additive Manufacturing*, 2017. (Cited on page 10.)

[28] Bey Vrancken, Victoria Cain, Rob Knutsen, and Jan Van Humbeeck. Residual stress via the contour method in compact tension specimens produced via selective laser melting. *Scripta Materialia*, 87:29–32, 2014. (Cited on page 10.)

[29] M. Shiomi, K. Osakada, K. Nakamura, T. Yamashita, and F. Abe. Residual Stress within Metallic Model Made by Selective Laser Melting Process. *CIRP Annals - Manufacturing Technology*, 53(1):195–198, 2004. (Cited on page 11.)

[30] Kwai S. Chan, Marie Koike, Robert L. Mason, and Toru Okabe. Fatigue life of titanium alloys fabricated by additive layer manufacturing techniques for dental implants. *Metallurgical and Materials Transactions A: Physical Metallurgy and Materials Science*, 44(2):1010–1022, 2013. (Cited on page 11.)

[31] F. Calignano, D. Manfredi, E. P. Ambrosio, L. Iuliano, and P. Fino. Influence of process parameters on surface roughness of aluminum parts produced by DMLS. *International Journal of Advanced Manufacturing Technology*, 67(9-12):2743–2751, 2013. (Cited on pages 11 and 12.)

[32] Giovanni Strano, Liang Hao, Richard M. Everson, and Kenneth E. Evans. Surface roughness analysis, modelling and prediction in selective laser melting. *Journal of Materials Processing Technology*, 213(4):589–597, 2013. (Cited on page 11.)

[33] Andrew Triantaphyllou, Claudiu L. Giusca, Gavin D. Macaulay, Felix Roerig, Matthias Hoebel, Richard K. Leach, Ben Tomita, and Katherine A. Milne. Surface texture measurement for additive manufacturing. *Surface Topography: Metrology and Properties*, 3(2), 2015. (Cited on pages 11 and 12.)

[34] H. Khalid Rafi, Thomas L. Starr, and Brent E. Stucker. A comparison of the tensile, fatigue, and fracture behavior of Ti-6Al-4V and 15-5 PH stainless steel parts made by selective laser melting. *International Journal of Advanced Manufacturing Technology*, 69(5-8):1299–1309, 2013. (Cited on page 12.)

[35] P. Edwards and M. Ramulu. Fatigue performance evaluation of selective laser melted Ti-6Al-4V. *Materials Science and Engineering A*, 598:327–337, 2014. (Cited on page 12.)

[36] Galina Kasperovich and Joachim Hausmann. Improvement of fatigue resistance and ductility of TiAl6V4 processed by selective laser melting. *Journal of Materials Processing Technology*, 220:202–214, 2015. (Cited on pages 12 and 13.)

[37] Grzegorz Pyka, Andrzej Burakowski, Greet Kerckhofs, Maarten Moesen, Simon Van Bael, Jan Schrooten, and Martine Wevers. Surface modification of Ti6Al4V open porous structures produced by additive manufacturing. *Advanced Engineering Materials*, 14(6):363–370, 2012. (Cited on page 12.)

[38] Pawan Tyagi, Tobias Goulet, Christopher Riso, Robert Stephenson, Nitt Chuenprateep, Justin Schlitzer, Cordell Benton, and Francisco Garcia-Moreno. Reducing the roughness of internal surface of an additive manufacturing produced 316 steel component by chempolishing and electropol-

ishing. *Additive Manufacturing*, 25(October 2018):32–38, 2019. (Cited on page 12.)

[39] Filippo Zanini, Elia Sbettega, Marco Sorgato, and Simone Carmignato. New Approach for Verifying the Accuracy of X-ray Computed Tomography Measurements of Surface Topographies in Additively Manufactured Metal Parts. *Journal of Nondestructive Evaluation*, 38(1), 2019. (Cited on pages 12 and 13.)

[40] Simone Carmignato, Valentina Aloisi, Fabrizio Medeossi, Filippo Zanini, and Enrico Savio. Influence of surface roughness on computed tomography dimensional measurements. *CIRP Annals - Manufacturing Technology*, 66(1):499–502, 2017. (Cited on pages 12 and 22.)

[41] Jacob C. Snyder, Curtis K. Stimpson, Karen a. Thole, and Dominic J. Mongillo. Build Direction Effects on Microchannel Tolerance and Surface Roughness. *Journal of Mechanical Design*, 137(11):111411, 2015. (Cited on page 12.)

[42] Greet Kerckhofs, Grzegorz Pyka, Maarten Moesen, Simon Van Bael, Jan Schrooten, and Martine Wevers. High-resolution microfocus X-ray computed tomography for 3d surface roughness measurements of additive manufactured porous materials. *Advanced Engineering Materials*, 15(3):153–158, 2013. (Cited on page 12.)

[43] Andrew Townsend, Liam Blunt, and Paul J. Bills. Investigating the capability of microfocus x-ray computed tomography for areal surface analysis of additively manufactured parts. In *American Society for Precision Engineering Summer Topical Meeting: Dimensional Accuracy and Surface Finish in Additive Manufacturing*, 2016. (Cited on page 13.)

[44] Agustin Diaz, Lane Winkelmann, Justin Michaud, and Cesar Terrazas. Surface finishing and characterization of titanium additive manufacturing components: From rich to smooth surface. In *European Congress and Exhibition on Powder Metallurgy. European PM Conference Proceedings*, pages 1–6. The European Powder Metallurgy Association, 2016. (Cited on page 13.)

[45] Andrew Townsend, Radu Racasan, Richard Leach, Nicola Senin, Adam Thompson, Andrew Ramsey, David Bate, Peter Woolliams, Stephen Brown, and Liam Blunt. An interlaboratory comparison of X-ray computed tomography measurement for texture and dimensional characterisation of additively manufactured parts. *Additive Manufacturing*, 23(September):422–432, 2018. (Cited on page 13.)

[46] International Organization for Standardization. ISO 25178-2:2012(E) Geometrical product specifications (GPS) Surface texture: Areal , 2012. (Cited on page 13.)

[47] Ondrej Koukal, Daniel Koutny, David Palousek, Radek Vrana, Tomas Zikmund, and Libor Pantelejev. Research about the Influence of Process Parameters of Selective Laser Melting on Material EN AW 2618. *Proceedings of Euro PM 2015*, pages 1–6, 2015. (Cited on page 13.)

[48] Nesma T. Aboulkhair, Nicola M. Everitt, Ian Ashcroft, and Chris Tuck. Reducing porosity in AlSi10Mg parts processed by selective laser melting. *Additive Manufacturing*, 1:77–86, 2014. (Cited on page 13.)

[49] M. Suard, G. Martin, P. Lhuissier, R. Dendievel, F. Vignat, J. J. Blandin, and F. Villeneuve. Mechanical equivalent diameter of single struts for the stiffness prediction of lattice structures produced by Electron Beam Melting. *Additive Manufacturing*, 8:124–131, 2015. (Cited on page 13.)

[50] M.H. Too, K.F. Leong, C.K. Chua, Z.H. Du, S.F. Yang, C.M. Cheah, and S.L. Ho. Investigation of 3D non-random porous structures by fused deposition modelling. *The International Journal of Advanced Manufacturing Technology*, 19(3):217–223, 2002. (Cited on page 15.)

[51] A. Boschetto and L. Bottini. Accuracy prediction in fused deposition modeling. *International Journal of Advanced Manufacturing Technology*, 73(5-8):913–928, 2014. (Cited on page 15.)

[52] Thomas Pfeifer, Carsten Koch, Luke Van Hulle, Gerardo A Mazzei Capote, and Natalie Rudolph. Optimization of the FDM Additive Manufacturing Process. *Proceedings of the Annual Technical Conference (ANTEC) of the Society of Plastics Engineers, Indianapolis*, pages 22–29, 2016. (Cited on page 15.)

[53] Q. Sun, G.M. Rizvi, C.T. Bellehumeur, and P. Gu. Effect of processing conditions on the bonding quality of FDM polymer filaments. *Rapid Prototyping Journal*, 14(2):72–80, 2008. (Cited on page 15.)

[54] Mahdi Kaveh, Mohsen Badrossamay, Ehsan Foroozmehr, and Ardeshir Hemasian Etefagh. Optimization of the printing parameters affecting dimensional accuracy and internal cavity for HIPS material used in fused deposition modeling processes. *Journal of Materials Processing Technology*, 226:280–286, 2015. (Cited on page 15.)

[55] Pavel Müller, Angela Cantatore, Jan L. Andreasen, Jochen Hiller, and Leonardo De Chiffre. Computed tomography as a tool for tolerance verification of industrial parts. *Procedia CIRP*, 10:125–132, 2013. (Cited on page 16.)

[56] Pierre A. Picouet, Fabiana Teran, Marina Gispert, and Maria Font i Furnols. Lean content prediction in pig carcasses, loin and ham by computed tomography (CT) using a density model. *Meat Science*, 86(3):616–622, 2010. (Cited on page 16.)

[57] Letitia Schoeman, Paul Williams, Anton du Plessis, and Marena Manley. X-ray micro-computed tomography (µCT) for non-destructive characterisation of food microstructure. *Trends in Food Science and Technology*, 47:10–24, 2016. (Cited on page 16.)

[58] Ralf Christoph and Hans Joachim Neumann. *X-ray tomography in industrial metrology*. Verlag Moderne Industrie, 2012. (Cited on pages 16 and 23.)

[59] A. Weck, D. S. Wilkinson, E. Maire, and H. Toda. Visualization by X-ray tomography of void growth and coalescence leading to fracture in model materials. *Acta Materialia*, 56(12):2919–2928, 2008. (Cited on page 16.)

[60] Hedi Nouri, Sofiane Guessasma, and Sofiane Belhabib. Structural imperfections in additive manufacturing perceived from the X-ray micro-tomography perspective. *Journal of Materials Processing Technology*, 234:113–124, 2016. (Cited on page 16.)

[61] S. Truscello, G. Kerckhofs, S. Van Bael, G. Pyka, J. Schrooten, and H. Van Oosterwyck. Prediction of permeability of regular scaffolds for skeletal tissue engineering: A combined computational and experimental study. *Acta Biomaterialia*, 8(4):1648–1658, 2012. (Cited on page 16.)

[62] Grzegorz Pyka, Greet Kerckhofs, Jan Schrooten, and Martine Wevers. The effect of spatial micro-CT image resolution and surface complexity on the morphological 3D analysis of open porous structures. *Materials Characterization*, 87:104–115, 2014. (Cited on page 16.)

[63] G Poludniowski, G Landry, F DeBlois, P M Evans, and F Verhaegen. SpekCalc: a program to calculate photon spectra from tungsten anode x-ray tubes. *Physics in Medicine and Biology*, 54(19):N433–N438, 2009. (Cited on page 17.)

[64] A. M. Cormack. Reconstruction of densities from their projections, with applications in radiological physics. *Physics in Medicine and Biology*, 18(2):195–207, 1973. (Cited on page 18.)

[65] Ehsan Samei. Performance of digital radiographic detectors: quantification and assessment methods. pages 37–47. 2003. (Cited on page 21.)

[66] Z Zhao, G J Gang, and J H Siewerdsen. Noise, sampling, and the number of projections in cone-beam CT with a flat-panel detector. *Medical physics*, 41(6):061909, 2014. (Cited on page 22.)

[67] P. Schuetz, I. Jerjen, J. Hofmann, M. Plamondon, A. Flisch, and U. Sennhauser. Correction algorithm for environmental scattering in industrial computed tomography. *NDT and E International*, 64:59–64, 2014. (Cited on page 22.)

[68] Ming Chang, Yongshun Xiao, Zhiqiang Chen, Liang Li, and Li Zhang. Preliminary study of rotary motion blurs in a novel industry ct imaging system. In *2011 IEEE Nuclear Science Symposium Conference Record*, pages 1358–1361. IEEE, 2011. (Cited on page 23.)

[69] Nobuyuki Otsu. A threshold selection method from gray-level histograms. *IEEE transactions on systems, man, and cybernetics*, 9(1):62–66, 1979. (Cited on page 23.)

[70] Carsten Bellon and Rüdiger Jaenisch, Gerd. aRTist, Analytical RT Inspection Simulation Tool for Industrial Application. *World Conference on Nondestructive Testing*, pages 25–28, 2008. (Cited on page 23.)

[71] Uwe Hilpert, Markus Bartscher, and Michael Neugebauer. Simulation-aided computed tomography (CT) for dimensional measurements. *International Symposium on Digital Industrial Radiology and Computed Tomography*, pages 1–15, 2007. (Cited on page 23.)

[72] Simone Carmignato. Accuracy of industrial computed tomography measurements: Experimental results from an international comparison. *CIRP Annals - Manufacturing Technology*, 61(1):491–494, 2012. (Cited on page 24.)

[73] J. M. Boone, J. A. Brink, S. Edyvean, W. Huda, W. Leitz, C. H. McCollough, and M. F. McNitt-Gray. Spatial Resolution in CT. *Journal of the ICRU*, 12(1):107–120, 2012. (Cited on page 24.)

[74] Markus Bartscher, Jens Illemann, and Ulrich Neuschaefer-Rube. ISO test survey on material influence in dimensional computed tomography. *Case Studies in Nondestructive Testing and Evaluation*, 6:79–92, 2016. (Cited on page 24.)

[75] Alexandra Kraemer and Gisela Lanza. Assessment of the Measurement Procedure for Dimensional Metrology with X-ray Computed Tomography. *Procedia CIRP*, 43:362–367, 2016. (Cited on page 24.)

[76] Markus Baier, Filippo Zanini, Enrico Savio, and Simone Carmignato. A new conversion approach between different characterization methods to measure the spot size of micro computed tomography systems. 06 2018. (Cited on page 24.)

[77] JIMA. Japan inspection instruments manufacturers association, 2019. (Cited on page 24.)

[78] QRM GmbH. Quality assurance in radiology and medicine, 2019. (Cited on page 24.)

[79] Ultimaker. Technical data sheet PLA Version 3.003. Technical report, 2016. (Cited on page 25.)

[80] International Organization for Standardization. ISO 527-2:2012 Plastics – Determination of tensile properties – Part 2: Test conditions for moulding and extrusion plastics, 2012. (Cited on page 25.)

[81] EOS GmbH. Material data sheet EOS Ti-6Al-4V powder, 2011. (Cited on page 26.)

[82] EOS. Material data sheet EOS Aluminium AlSi10Mg for EOSINT M 270, 2014. (Cited on pages 26 and 29.)

[83] EOS Gmbh. EOS M 290: The Benchmark for the Additive Manufacturing of High -Quality Metal Parts, 2018. (Cited on page 26.)

[84] International Organization for Standardization. ISO 6892-1:2016 Metallic materials, Tensile testing, Part 1: Method of test at room temperature, 2016. (Cited on page 29.)

Publications *in the series*
Örebro Studies in Technology

1. Bergsten, Pontus (2001) *Observers and Controllers for Takagi – Sugeno Fuzzy Systems*. Doctoral Dissertation.

2. Iliev, Boyko (2002) *Minimum-time Sliding Mode Control of Robot Manipulators*. Licentiate Thesis.

3. Spännar, Jan (2002) *Grey box modelling for temperature estimation*. Licentiate Thesis.

4. Persson, Martin (2002) *A simulation environment for visual servoing*. Licentiate Thesis.

5. Boustedt, Katarina (2002) *Flip Chip for High Volume and Low Cost – Materials and Production Technology*. Licentiate Thesis.

6. Biel, Lena (2002) *Modeling of Perceptual Systems – A Sensor Fusion Model with Active Perception*. Licentiate Thesis.

7. Otterskog, Magnus (2002) *Produktionstest av mobiltelefonantenner i mod-växlande kammare*. Licentiate Thesis.

8. Tolt, Gustav (2003) *Fuzzy-Similarity-Based Low-level Image Processing*. Licentiate Thesis.

9. Loutfi, Amy (2003) *Communicating Perceptions: Grounding Symbols to Artificial Olfactory Signals*. Licentiate Thesis.

10. Iliev, Boyko (2004) *Minimum-time Sliding Mode Control of Robot Manipulators*. Doctoral Dissertation.

11. Pettersson, Ola (2004) *Model-Free Execution Monitoring in Behavior-Based Mobile Robotics*. Doctoral Dissertation.

12. Överstam, Henrik (2004) *The Interdependence of Plastic Behaviour and Final Properties of Steel Wire, Analysed by the Finite Element Metod*. Doctoral Dissertation.

13. Jennergren, Lars (2004) *Flexible Assembly of Ready-to-eat Meals*. Licentiate Thesis.

14. Jun, Li (2004) *Towards Online Learning of Reactive Behaviors in Mobile Robotics*. Licentiate Thesis.

15. Lindquist, Malin (2004) *Electronic Tongue for Water Quality Assessment*. Licentiate Thesis.

16. Wasik, Zbigniew (2005) *A Behavior-Based Control System for Mobile Manipulation*. Doctoral Dissertation.

17. Berntsson, Tomas (2005) *Replacement of Lead Baths with Environment Friendly Alternative Heat Treatment Processes in Steel Wire Production*. Licentiate Thesis.

18. Tolt, Gustav (2005) *Fuzzy Similarity-based Image Processing*. Doctoral Dissertation.

19. Munkevik, Per (2005) *"Artificial sensory evaluation – appearance-based analysis of ready meals"*. Licentiate Thesis.

20. Buschka, Pär (2005) *An Investigation of Hybrid Maps for Mobile Robots*. Doctoral Dissertation.

21. Loutfi, Amy (2006) *Odour Recognition using Electronic Noses in Robotic and Intelligent Systems*. Doctoral Dissertation.

22. Gillström, Peter (2006) *Alternatives to Pickling; Preparation of Carbon and Low Alloyed Steel Wire Rod*. Doctoral Dissertation.

23. Li, Jun (2006) *Learning Reactive Behaviors with Constructive Neural Networks in Mobile Robotics*. Doctoral Dissertation.

24. Otterskog, Magnus (2006) *Propagation Environment Modeling Using Scattered Field Chamber*. Doctoral Dissertation.

25. Lindquist, Malin (2007) *Electronic Tongue for Water Quality Assessment*. Doctoral Dissertation.

26. Cielniak, Grzegorz (2007) *People Tracking by Mobile Robots using Thermal and Colour Vision*. Doctoral Dissertation.

27. Boustedt, Katarina (2007) *Flip Chip for High Frequency Applications – Materials Aspects*. Doctoral Dissertation.

28. Soron, Mikael (2007) *Robot System for Flexible 3D Friction Stir Welding*. Doctoral Dissertation.

29. Larsson, Sören (2008) *An industrial robot as carrier of a laser profile scanner. – Motion control, data capturing and path planning*. Doctoral Dissertation.

30. Persson, Martin (2008) *Semantic Mapping Using Virtual Sensors and Fusion of Aerial Images with Sensor Data from a Ground Vehicle*. Doctoral Dissertation.

31. Andreasson, Henrik (2008) *Local Visual Feature based Localisation and Mapping by Mobile Robots*. Doctoral Dissertation.

32. Bouguerra, Abdelbaki (2008) *Robust Execution of Robot Task-Plans: A Knowledge-based Approach*. Doctoral Dissertation.

33. Lundh, Robert (2009) *Robots that Help Each Other: Self-Configuration of Distributed Robot Systems.* Doctoral Dissertation.

34. Skoglund, Alexander (2009) *Programming by Demonstration of Robot Manipulators.* Doctoral Dissertation.

35. Ranjbar, Parivash (2009) *Sensing the Environment: Development of Monitoring Aids for Persons with Profound Deafness or Deafblindness.* Doctoral Dissertation.

36. Magnusson, Martin (2009) *The Three-Dimensional Normal-Distributions Transform – an Efficient Representation for Registration, Surface Analysis, and Loop Detection.* Doctoral Dissertation.

37. Rahayem, Mohamed (2010) *Segmentation and fitting for Geometric Reverse Engineering. Processing data captured by a laser profile scanner mounted on an industrial robot.* Doctoral Dissertation.

38. Karlsson, Alexander (2010) *Evaluating Credal Set Theory as a Belief Framework in High-Level Information Fusion for Automated Decision-Making.* Doctoral Dissertation.

39. LeBlanc, Kevin (2010) *Cooperative Anchoring – Sharing Information About Objects in Multi-Robot Systems.* Doctoral Dissertation.

40. Johansson, Fredrik (2010) *Evaluating the Performance of TEWA Systems.* Doctoral Dissertation.

41. Trincavelli, Marco (2010) *Gas Discrimination for Mobile Robots.* Doctoral Dissertation.

42. Cirillo, Marcello (2010) *Planning in Inhabited Environments: Human-Aware Task Planning and Activity Recognition.* Doctoral Dissertation.

43. Nilsson, Maria (2010) *Capturing Semi-Automated Decision Making: The Methodology of CASADEMA.* Doctoral Dissertation.

44. Dahlbom, Anders (2011) *Petri nets for Situation Recognition.* Doctoral Dissertation.

45. Ahmed, Muhammad Rehan (2011) *Compliance Control of Robot Manipulator for Safe Physical Human Robot Interaction.* Doctoral Dissertation.

46. Riveiro, Maria (2011) *Visual Analytics for Maritime Anomaly Detection.* Doctoral Dissertation.

47. Rashid, Md. Jayedur (2011) *Extending a Networked Robot System to Include Humans, Tiny Devices, and Everyday Objects*. Doctoral Dissertation.

48. Zain-ul-Abdin (2011) *Programming of Coarse-Grained Reconfigurable Architectures*. Doctoral Dissertation.

49. Wang, Yan (2011) *A Domain-Specific Language for Protocol Stack Implementation in Embedded Systems*. Doctoral Dissertation.

50. Brax, Christoffer (2011) *Anomaly Detection in the Surveillance Domain*. Doctoral Dissertation.

51. Larsson, Johan (2011) *Unmanned Operation of Load-Haul-Dump Vehicles in Mining Environments*. Doctoral Dissertation.

52. Lidström, Kristoffer (2012) *Situation-Aware Vehicles: Supporting the Next Generation of Cooperative Traffic Systems*. Doctoral Dissertation.

53. Johansson, Daniel (2012) *Convergence in Mixed Reality-Virtuality Environments. Facilitating Natural User Behavior*. Doctoral Dissertation.

54. Stoyanov, Todor Dimitrov (2012) *Reliable Autonomous Navigation in Semi-Structured Environments using the Three-Dimensional Normal Distributions Transform (3D-NDT)*. Doctoral Dissertation.

55. Daoutis, Marios (2013) *Knowledge Based Perceptual Anchoring: Grounding percepts to concepts in cognitive robots*. Doctoral Dissertation.

56. Kristoffersson, Annica (2013) *Measuring the Quality of Interaction in Mobile Robotic Telepresence Systems using Presence, Spatial Formations and Sociometry*. Doctoral Dissertation.

57. Memedi, Mevludin (2014) *Mobile systems for monitoring Parkinson's disease*. Doctoral Dissertation.

58. König, Rikard (2014) *Enhancing Genetic Programming for Predictive Modeling*. Doctoral Dissertation.

59. Erlandsson, Tina (2014) *A Combat Survivability Model for Evaluating Air Mission Routes in Future Decision Support Systems*. Doctoral Dissertation.

60. Helldin, Tove (2014) *Transparency for Future Semi-Automated Systems. Effects of transparency on operator performance, workload and trust*. Doctoral Dissertation.

61. Krug, Robert (2014) *Optimization-based Robot Grasp Synthesis and Motion Control*. Doctoral Dissertation.

62. Reggente, Matteo (2014) *Statistical Gas Distribution Modelling for Mobile Robot Applications*. Doctoral Dissertation.

63. Längkvist, Martin (2014) *Modeling Time-Series with Deep Networks*. Doctoral Dissertation.

64. Hernández Bennetts, Víctor Manuel (2015) *Mobile Robots with In-Situ and Remote Sensors for Real World Gas Distribution Modelling*. Doctoral Dissertation.

65. Alirezaie, Marjan (2015) *Bridging the Semantic Gap between Sensor Data and Ontological Knowledge*. Doctoral Dissertation.

66. Pashami, Sepideh (2015) *Change Detection in Metal Oxide Gas Sensor Signals for Open Sampling Systems*. Doctoral Dissertation.

67. Lagriffoul, Fabien (2016) *Combining Task and Motion Planning*. Doctoral Dissertation.

68. Mosberger, Rafael (2016) *Vision-based Human Detection from Mobile Machinery in Industrial Environments*. Doctoral Dissertation.

69. Mansouri, Masoumeh (2016) *A Constraint-Based Approach for Hybrid Reasoning in Robotics*. Doctoral Dissertation.

70. Albitar, Houssam (2016) *Enabling a Robot for Underwater Surface Cleaning*. Doctoral Dissertation.

71. Mojtahedzadeh, Rasoul (2016) *Safe Robotic Manipulation to Extract Objects from Piles: From 3D Perception to Object Selection*. Doctoral Dissertation.

72. Köckemann, Uwe (2016) *Constraint-based Methods for Human-aware Planning*. Doctoral Dissertation.

73. Jansson, Anton (2016) *Only a Shadow. Industrial Computed Tomography Investigation, and Method Development, Concerning Complex Material Systems*. Licentiate Thesis.

74. Sebastian Hällgren (2017) *Some aspects on designing for metal Powder Bed Fusion*. Licentiate Thesis.

75. Junges, Robert (2017) *A Learning-driven Approach for Behavior Modeling in Agent-based Simulation*. Doctoral Dissertation.

76. Ricão Canelhas, Daniel (2017) *Truncated Signed Distance Fields Applied To Robotics*. Doctoral Dissertation.

77. Asadi, Sahar (2017) *Towards Dense Air Quality Monitoring: Time-Dependent Statistical Gas Distribution Modelling and Sensor Planning.* Doctoral Dissertation.

78. Banaee, Hadi (2018) *From Numerical Sensor Data to Semantic Representations: A Data-driven Approach for Generating Linguistic Descriptions.* Doctoral Dissertation.

79. Khaliq, Ali Abdul (2018) *From Ants to Service Robots: an Exploration in Stigmergy-Based Navigation Algorithms.* Doctoral Dissertation.

80. Kucner, Tomasz Piotr (2018) *Probabilistic Mapping of Spatial Motion Patterns for Mobile Robots.* Doctoral Dissertation.

81. Dandan, Kinan (2019) *Enabling Surface Cleaning Robot for Large Food Silo.* Doctoral Dissertation.

82. El Amine, Karim (2019) *Approaches to increased efficiency in cold drawing of steel wires.* Licentiate Thesis.

83. Persson, Andreas (2019) *Studies in Semantic Modeling of Real-World Objects using Perceptual Anchoring.* Doctoral Dissertation.

84. Jansson, Anton (2019) *More Than a Shadow. Computed Tomography Method Development and Applications Concerning Complex Material Systems.* Doctoral Dissertation.

85. Zekavat, Amir Reza (2019) *Application of X-ray Computed Tomography for Assessment of Additively Manufactured Products.* Doctoral Dissertation.